

NAVAL POSTGRADUATE SCHOOL

Monterey, California



THESIS

CHARACTERIZATION OF SUBMERGED-ARC AND
GAS-METAL-ARC WELDMENTS IN HY-100 STEEL

by

Alfred E. Therrien

December 1983

Thesis Advisor:

K. D. Challenger

Approved for public release; distribution unlimited.

T215703

REPORT DOCUMENTATION PAGE

READ INSTRUCTIONS
BEFORE COMPLETING FORM

1. REPORT NUMBER

2. GOVT ACCESSION NO.

3. RECIPIENT'S CATALOG NUMBER

4. TITLE (and Subtitle)

Characterization of Submerged-Arc and
Gas-Metal-Arc Weldments in HY-100 Steel

5. TYPE OF REPORT & PERIOD COVERED

Master's Thesis
December 1983

6. PERFORMING ORG. REPORT NUMBER

7. AUTHOR(s)

Alfred E. Therrien

8. CONTRACT OR GRANT NUMBER(s)

9. PERFORMING ORGANIZATION NAME AND ADDRESS

Naval Postgraduate School
Monterey, California 93943

10. PROGRAM ELEMENT, PROJECT, TASK
AREA & WORK UNIT NUMBERS

11. CONTROLLING OFFICE NAME AND ADDRESS

Naval Postgraduate School
Monterey, California 93943

12. REPORT DATE

December 1983

13. NUMBER OF PAGES

82

14. MONITORING AGENCY NAME & ADDRESS (if different from Controlling Office)

15. SECURITY CLASS. (of this report)

Unclassified

15a. DECLASSIFICATION/DOWNGRADING
SCHEDULE

16. DISTRIBUTION STATEMENT (of this Report)

Approved for public release; distribution unlimited.

17. DISTRIBUTION STATEMENT (of the abstract entered in Block 20, if different from Report)

18. SUPPLEMENTARY NOTES

19. KEY WORDS (Continue on reverse side if necessary and identify by block number)

microstructure	ductile-to-brittle transition temperature
bainite	inclusions
martensite	cooling rate
toughness	

20. ABSTRACT (Continue on reverse side if necessary and identify by block number)

Unsatisfactory weld toughness in submerged arc welded (SAW) HY-100 steel weldments precludes this process from large scale HY-100 shipbuilding production efforts. The gas metal arc welding (GMAW) process produces acceptable weldments in HY-100 steel. Optical, scanning electron and transmission electron microscopy were utilized to characterize and compare the microstructures in the last pass in each weldment for each process. The SAW weldment contains a coarse-upper bainitic

20. ABSTRACT (Continued)

microstructure and the GMAW weldment contains a martensitic structure. The cooling rate in the SAW was 42% slower than in GMAW. The SAW contained 25% more weld metal inclusions than the GMAW. Microhardness traverses were conducted and the profiles reflect significantly lower microhardness in the untempered last pass weld metal of SAW weldment, but the tempered weld metal microhardness in both weldments was measured at 250 HV. Charpy impact tests were conducted and impact transition curves were developed revealing that the SAW weldments ductile-to-brittle transition temperature was 50°C higher than the GMAW weldment.

Approved for public release; distribution unlimited.

Characterization of Submerged-Arc and Gas-Metal-Arc
Weldments in HY-100 Steel

by

Alfred E. Therrien
Lieutenant Commander, United States Navy
B.S. Eng., Maine Maritime Academy, 1971

Submitted in partial fulfillment of the
requirements for the degree of

MASTER OF SCIENCE IN ENGINEERING SCIENCE

from the

NAVAL POSTGRADUATE SCHOOL
December 1983

TABLE OF CONTENTS

I.	INTRODUCTION	9
II.	BACKGROUND	11
III.	EXPERIMENTAL PROCEDURE	21
IV.	EXPERIMENTAL RESULTS	35
V.	DISCUSSION	68
VI.	SUMMARY AND CONCLUSIONS	77
VII.	RECOMMENDATIONS	79
	LIST OF REFERENCES	80
	INITIAL DISTRIBUTION LIST	82

LIST OF FIGURES

1.	Time-Temperature-Transformation Curves for HY-80 .	16
2.	GMAW Process Parameters and Weld Pass Sequence . .	22
3.	SAW Process Parameters and Weld Pass Sequence . .	23
4.	Photo of GMAW Macroetched Specimen	26
5.	Photo of SAW Macroetched Specimen	27
6.	GMAW Microhardness Traverses	28
7.	SAW Microhardness Traverses	29
8.	Sectioned Last Pass in GMAW Showing Wafer Cutting Technique and TEM Foil Location	32
9.	Sectioned Last Pass in SAW Showing Wafer Cutting Technique and TEM Foil Locations	33
10(a)	Vickers Hardness Traverse A-1 (GMAW)	37
(b)	Vickers Hardness Traverse A-5 (GMAW)	38
(c)	Vickers Hardness Traverse A-4 (GMAW)	39
(d)	Vickers Hardness Traverse A-2 (GMAW)	40
(e)	Vickers Hardness Traverse A-3 (GMAW)	41
11(a)	Vickers Hardness Traverse B-1 (SAW)	43
(b)	Vickers Hardness Traverse B-4 (SAW)	44
(c)	Vickers Hardness Traverse B-3 (SAW)	45
(d)	Vickers Hardness Traverse B-2 (SAW)	46
12.	Microhardness Traverses A-3 (GMAW) and B-2 (SAW) .	47
13.	GMAW Ductile-to-Brittle Transition Temperature Curve	50
14.	SAW Ductile-to-Brittle Transition Temperature Curve	51

15.	GMAW and SAW Ductile-to-Brittle Transition Temperature Curves	52
16.	Optical Micrographs of GMAW and SAW Weldments in Last Passes	53
17.	Optical Dark Field and TEM Microphotographs of GMAW in Last Pass Showing Typical Inclusion Distribution	54
18.	Optical Dark Field and TEM Microphotographs of SAW in Last Pass Showing Typical Inclusion Distribution	55
19.	SEM Micrograph of HY-100 Base Metal	57
20.	SEM Micrographs of Various Regions of the Last Pass in GMAW and SAW Weldments	58
21.	TEM Micrographs of GMAW and SAW Weldments in Upper Weld Region of Last Pass	60
22.	TEM Micrograph of Type II Bainite with Fine Cementite Particles Distributed in Ferrite Laths Located in the Upper Weld Region of SAW Weldment . .	62
23.	TEM Micrographs of GMAW and SAW Weldments in Coarse Grained HAZ of Last Pass	63
24.	SEM Micrographs of Ductile Fracture Surfaces in GMAW and SAW Weldments	65
25.	SEM Micrographs of Brittle Fracture Surfaces in GMAW and SAW Weldments	66
26.	Yield and Fracture Strength and Fracture Strain Dependence on Grain Size in Low Carbon Steel at -196°C	73
27.	Dependence of Transition Temperature on Grain Size	74

ACKNOWLEDGEMENTS

I wish to express my sincere appreciation to my thesis advisor, Professor Ken Challenger, for his valuable guidance in this research effort. I would also like to thank Dr. Prabir Deb, whose advice, support and friendship truly made my research enjoyable. I cannot forget Mr. Tom Kellogg whose assistance in the laboratory, I could have never survived without. Last but certainly not least, I want to thank my wife, Janet and our two daughters, Alicia and Jana for their patience and understanding during these past three years.

I wish to dedicate this research to my mother Jacqueline and my father Robert. Their concern, support and love has always been with me and I know it always will. More than anyone, they deserve the credit for the contentment and fullness I feel today!

I. INTRODUCTION

Research on HY-100 steel weldments continues in order to provide the Navy with a material which can improve upon the current excellent properties of HY-80 steel. HY-100 steel could in fact improve upon the strength-weight ratio and fracture toughness currently realized in submarine hull structures made of HY-80. This appears to be the goal of current research being conducted with HY-100 steels. HY-100 steel applications, heretofore, have been limited to portions of aircraft carrier flight decks.

A significant portion of the cost of ship construction is attributed to welding. It has been estimated as high as 50% of the total manhours spent in hull fabrication is associated with welding, and this is due primarily to the labor intensive nature of welding. The cost effectiveness of highly automated, high speed and high deposition rate welding processes make them very desirable. The submerged arc welding (SAW) process falls in this category. SAW has been in wide use throughout industry for many years, in fact nearly 15% of the total carbon steel weld metal in the U.S. is deposited by submerged arc welding [Ref. 1].

One of the major problems preventing HY-100 from being used in large scale shipbuilding projects is the general degradation in its weldment properties when welded with

SAW, marked by unacceptable fracture resistance at low temperatures. There is very little if any published literature on the structure and mechanical properties of HY-100 weldments.

It was decided that this research would begin by the characterization of HY-100 submerged arc weldments and HY-100 gas metal arc weldment (GMAW). It was felt that since the HY-100 GMAW produced acceptable weld properties and that the HY-100 SAW did not, that a comparison between the two characterized weldments could produce valuable insight which could eventually lead to the resolution of this problem.

II. BACKGROUND

HY-100 is a high-strength quenched and tempered steel approved for use by the U.S. Navy for construction of large ocean vessels. It is a low-carbon steel that achieves its strength and toughness through a quenching-and-tempering heat treatment. Additionally, HY-100 requires no post weld heat treatment when established welding procedures are followed. Welding procedures for HY-100 are governed by military specifications MIL-S-19322, [Ref. 2]. Production of HY-100 plate steel is governed by MIL-S-16216A, [Ref. 3]. The chemical composition limits of HY-100 are shown in Table 1.

The alloying elements each serve an important role in establishing the mechanical properties of HY-100. Carbon is maintained below 0.20% to ensure good weldability while achieving the desired strength levels. Nickel is added primarily to increase the hardenability. The limitation of sulphur and phosphorus content is required to minimize the detrimental effects of these elements during welding. Sulphur combines with iron to form iron-sulphide, which liquifies at normal rolling and forging temperatures. Manganese addition prevents the formation of iron-sulphide by preferentially forming manganese-sulphide thereby limiting the sulphur available for reaction with iron.

Table 1
Chemical Composition Limits of HY-100 Steel Plate

Element	MIL-S-16216 HY-100 (Percent)	Commercial A543 Trade B
Carbon	0.20 Max	0.23 Max
Manganese	0.10-0.40	0.40 Max
Silicon	0.15-0.35	0.20-0.35
Nickel	2.25-3.50	2.60-3.25
Chromium	1.00-1.80	1.5-2.0
Molybdenum	0.20-0.60	0.45-0.60
Phosphorus (a)	0.025 Max	0.02 Max
Sulphur (a)	0.025 Max	0.02 Max
Titanium	0.02 Max	-
Vanadium	0.03 Max	0.03 Max
Copper	0.25 Max	-
Iron	Remainder	Remainder

(a) The percent of combined phosphorus and sulphur shall be 0.045 Max.

The manganese also solid solution strengthens the steel, without reducing ductility. Excess manganese causes embrittlement so its content is restricted to a maximum of 0.40%. Molybdenum is used to increase the temper resistance, and to improving hardenability, creep resistance and machinability. Silicon is added to act as a deoxidizer. Chromium is added to increase hardenability and secondary hardening during the tempering treatment of HY-100. The limits are set between 1.0 to 1.80% to act as a carbide former in hardening the steel. Chromium and copper improves its corrosion resistance [Ref. 4].

HY-100 is a fully-killed, low alloy steel that attains a good combination of strength and toughness through quenching and tempering. The resulting microstructures of the as-received HY-100 is a combination of tempered bainite and tempered martensite throughout the plate. MIL-S-16216 lists only two limitations regarding the procedures for quenching and tempering heat treatments required in the production of HY-100 steel. The first is to establish the final tempering temperature as not less than 1050°F, and the second is that the mid-thickness microstructure shall contain not less than 80% martensite.

The mechanical property specification limits of HY-100 steel are shown in Table 2. Although a specific time-temperature-transformation (TTT) diagram has not been developed for HY-100, Emmanuel, Young and Spahr [Ref. 5]

Table 2

Mechanical Property Limits of HY-100 Steel Plate

Property	MIL-S-16216	A543 (Grade B)
Tensile strength ksi (MPa)	NS ^(a)	115/135/732/930
Yield strength (0.2% offset, ksi) (MPa)	100/115 ^(b) (689/732)	100 Min. (689)
Elongation in 2 in., min. percent	18 ^(b)	14
Reduction in area min. percent		
Longitudinal	50 ^(b)	NS
Transverse	45 ^(b)	NS
Charpy V-notch min. impact (ft-lbs) (J)		
1/2 to 2 in.	45 (67) @ -120°F (-84°C)	NS
over 2 in.	30 (40) @ -120°F (-84°C)	NS

(a) Not specified.

(b) These values for plate thicknesses 5/8 inch and over.

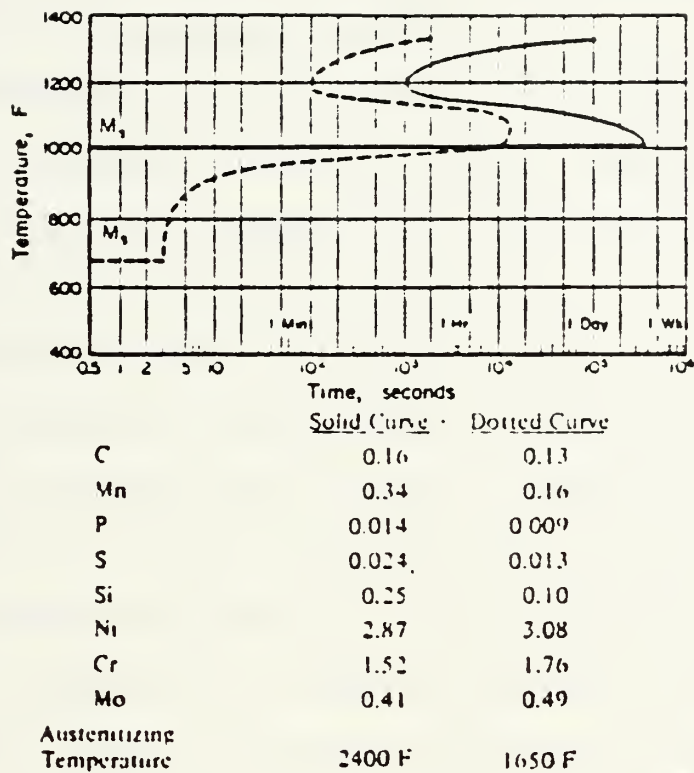
developed a TTT diagram for HY-80 steel (shown in Figure 1) which is very similar to HY-100 steel differing only in that HY-100 has a slightly higher carbon and nickel content.* Figure 1 illustrates the sluggishness of the austenite decomposition, and shows these transformations as a function of austenizing temperature. The slow response to transformation results in a duplex microstructure consisting of martensite and bainite, typically found in HY-80/100 steel plate.

Preheating HY-100 prior to welding is a standard welding practice. The minimum amount of preheat necessary is dependent on the plate thickness to be welded as shown in Table 3.

Table 3

Minimum Preheat Temperatures for Welding HY-100 Steel Plate

Plate Thickness (in.)	Minimum Preheat or Interpass Temperature (°F)
up to 1/2	75
1/2 to 1 1/8	125
over 1 1/8	200



Source: Published information in Reference 5.

Figure 1. Time-Temperature-Transformation Curves for HY-80

Preheating is necessary for the prevention of hydrogen entrapment in the weldment and to aid in preventing weld-metal cracking in restrained welds.

It is appropriate at this point to describe both the SAW and GMAW processes so that a clearer understanding can be reached as to the resulting weld microstructures generated by each of these two processes.

Submerged arc welding is an arc welding process wherein fusion is produced by heating with an electric arc between a bare metal electrode and the work. Pressure is not used and filler metal is obtained either from the electrode or from a supplementary welding rod. The welding zone is covered and shielded by a blanket of granular fusible material known as flux. Thus, the welding electrode at the arc end is completely covered at all times during the actual welding operation and the entire welding action takes place beneath a bath of molten flux. The flux is an essential feature of the submerged arc welding process. The flux, when cold, is a nonconductor of electricity, but in the molten state it becomes a highly conductive medium. The heat produced by the current flowing through the arc and conductive paths keeps the flux molten in the areas surrounding the deposited weld metal. The solidification temperature for fluxes is below that for steel so that adequate protection for the molten metal is always assured. The upper visible portion of the flux is not melted. It

remains unchanged in appearance and properties and it can be recovered and reused. During its molten state, the flux provides exceptionally suitable conditions for unusually high current intensities. Thus, great quantities of heat may be generated. The insulating qualities of flux enable the intense heat to be concentrated in a relatively small welding zone, where the welding electrode and base metal are rapidly fused. Generally two volumes of base metal are melted for each volume of filler metal. This also leads to very large Heat Affected Zones (HAZ).

Gas metal-arc welding (GMAW) is a gas shielded-arc welding process in which the welding heat is obtained from an arc between a consumable electrode and the workpiece. The filler wire (electrode) is melted in an inert gas atmosphere and is transferred to the joint where the arc provides sufficient heat to fuse the plate surfaces. The essentials are a torch through which the electrode is fed, a supply of inert shielding gas, a control for governing the wire feed through the torch, and a direct current power supply. A d-c reverse polarity power supply is normally used. This sets up a flow of electrons toward the electrode while the flow of positive ions is downwards toward the workpiece. The significant factor is that the large force exerted on the drops of metal by the positive gas ions is downward, which imparts a high velocity to the drops causing a very deep penetration, particularly at the center

of the weld area. So, this spray arc transfer of material through the protected arc column provides a highly efficient heat input, with a resultant high intensity heat source which permits rapid welding deep penetration and creates a relatively small HAZ.

SAW and GMAW are both fusion welding processes. The way in which a fusion weld is made may have a profound effect on the properties of joint. The three most important characteristics of a fusion-welding process in this respect are the intensity of the heat source, the heat input per unit length of weld and the type and effectiveness of the method used to shield the weld from the atmosphere. SAW is considered a high heat input process. Generally, this will have the effect of lowering the cooling rate across the weld metal and HAZ (insulating quality of flux also lowers cooling rate) and grains solidifying in weld metal grow coherently with grains in the solid metal (HAZ) at the fusion boundary. Since a longer time is spent above the grain-coarsening temperature, this would give rise to coarser block-like upper transformation temperature products both in the weld metal and in the HAZ. This would have the effect of reducing the notch ductility in both these regions. Also use of non-basic fluxes can increase the oxygen content in carbon steel and provide a larger concentration of microinclusion which would promote the formation of upper transformation temperature products and

thereby generate a coarser microstructure with a correspondingly lower notch-ductility [Ref. 6]. The GMAW on the other hand is considered a high heat intensity process and this will generally have the effect of increasing the cooling rate across the weld metal and HAZ. This would give rise to finer lower transformation temperature products such as martensite thereby raising the notch-ductility both in the weld metal and HAZ. In the GMAW an inert shielding gas is used to protect the molten weld metal and prevent it from interacting with the oxygen and nitrogen in the atmosphere. The inert shielding gases used in GMAW do not possess the potential for affecting weld properties as do the fluxes used in the SAW process.

III. EXPERIMENTAL PROCEDURES

A. MACROSAMPLE PREPARATION

Two HY-100 steel plates, each measuring one inch thick, twelve inches long by eight inches wide were prepared by the Naval Ship Research and Development Center, Annapolis, Maryland. Each plate contained a weld joint running longitudinally. The joints in each plate were single beveled at 60 degrees and a backing plate was tack welded to the base of each plate at the joint. One plate was welded using the GMAW process and the other using the SAW process. Figure 2 and Figure 3 list the process parameters and weld respectively. Identical electrode material was used in each welding process. Equal heat input rates were maintained for each process by varying voltage and travel speed. Electrode composition is listed in Table 4. The flux used in the SAW process had a basicity index of 3.1 and is considered a fully basic flux. The plates were then sectioned perpendicular to the weld with a horizontal band saw into approximately one half inch thick specimens. Each specimen face was cold sanded on a belt sander to produce a smooth, flat surface suitable for macroetching. A 2% Nital solution was used to macroetch the samples and expose the weld characteristics of each sample. Both the GMAW and SAW specimens were

Process: GMAW

Electrode: MIL-120S-1 (Linde 120, 3/32-inch diameter,
Heat 120011)

Shielding Gas: 98% argon--2% oxygen

Preheat/Interpass Temperature: 250°-275° F

Current: 400A

Voltage: 28V

Travel Speed: 12 ipm

Heat Input: 56.0 kJ/in (2.2 kJ/mm)

Cooling Rate at 1000° F by TC Plunge: Bead 7--32.8° F/sec
 Bead 13--33.9° F/sec
 Bead 16--35.0° F/sec
 Bead 17--35.4° F/sec

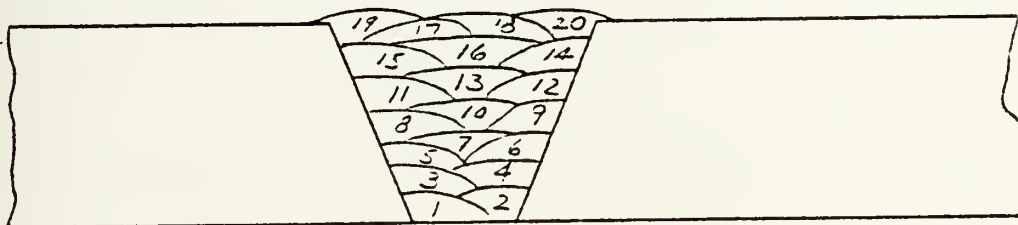


Figure 2 GMAW Process Parameters and Weld Pass Sequence

Process: SAW

Electrode: MIL-120S-1 (Linde 120, 3/32-inch diameter,
Heat 120011)

Flux: Oerlikon OP121TT, Lot 091013

Preheat/Interpass Temperature: 250°-275° F

Current: 400A

Voltage: 35V

Travel Speed: 15 ipm

Heat Input: 56.0 kJ/in (2.2 kJ/mm)

Cooling Rate at 1000° F by TC Plunge:

Bead	8--	23.2° F/sec
Bead	11--	17.6° F/sec
Bead	14--	21.8° F/sec
Bead	17--	18.9° F/sec

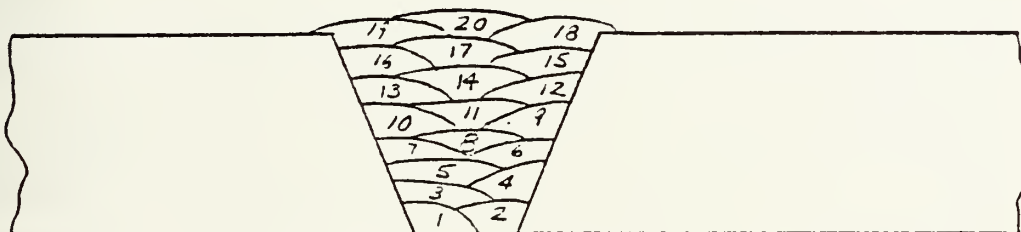


Figure 3 SAW Process Parameters and Weld Pass Sequence

Table 4
Chemical Composition of Linde 120 Electrode

Element	MIL-120S-1 (Percent)
Carbon	0.068
Manganese	1.56
Silicon	0.30
Phosphorus	0.009
Sulphur	0.006
Nickel	2.47
Molybdenum	0.50
Chromium	0.32
Vanadium	less than 0.01
Aluminum	less than 0.01
Titanium	less than 0.01
Zirconium	less than 0.01
Copper	0.02
Cobalt	0.06
Oxygen	131 ppm
Nitrogen	77 ppm

submerged for 10 minutes until the details of each weld became evident. Figures 4 and 5 illustrate the prepared macrosamples for each weldment.

B. HARDNESS TESTING

Samples suitable for metallographic examination and comparison were selected from various regions including the last pass region in each weldment. Samples were cut, mounted, polished and etched in 2% Nital for 20 seconds in order to locate regions of interest. In order to track microhardness measurements, a line was scribed across each region of interest, Figures 6 and 7. The samples were then polished lightly to remove the etch and Vickers microhardness measurements were made along each scribe using a diamond indenter and a 200 gram load. Penetrations were made at 0.1 mm intervals.

C. OPTICAL MICROSCOPY SAMPLE PREPARATION

The last pass region from each weldment was selected to be examined with a Zeiss Universal Photomicroscope. The last pass was chosen since it had not been thermally cycled by subsequent passes and would represent the least complex microstructures. Within the last pass, the upper weld region and the coarse-grained HAZ were selected to be characterized and compared. The specimens used for microhardness testing were used for this purpose after a 20 second etch in 2% Nital. These same samples were then polished to

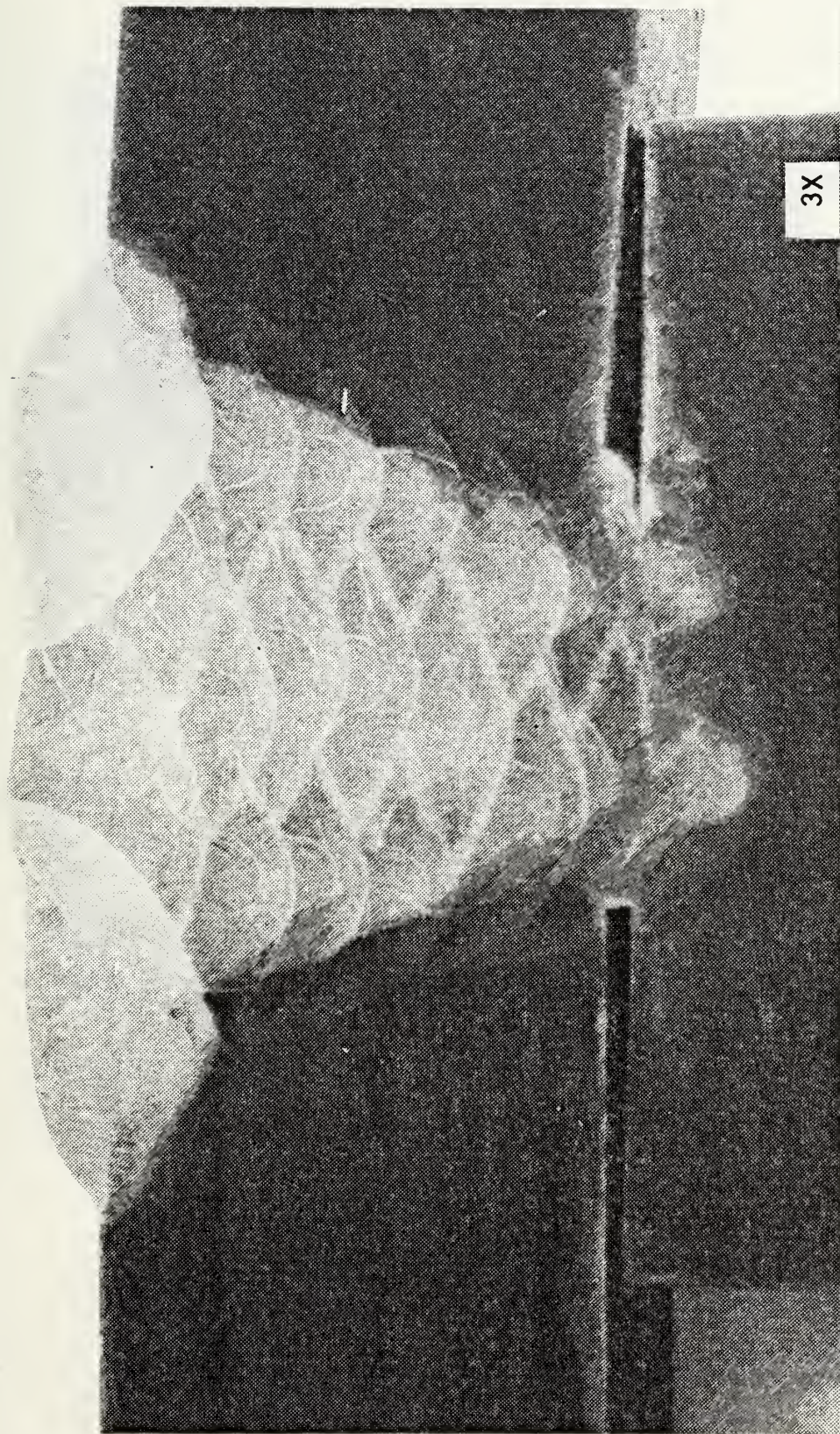


Figure 4 Photo of GMAW Macroetched Specimen

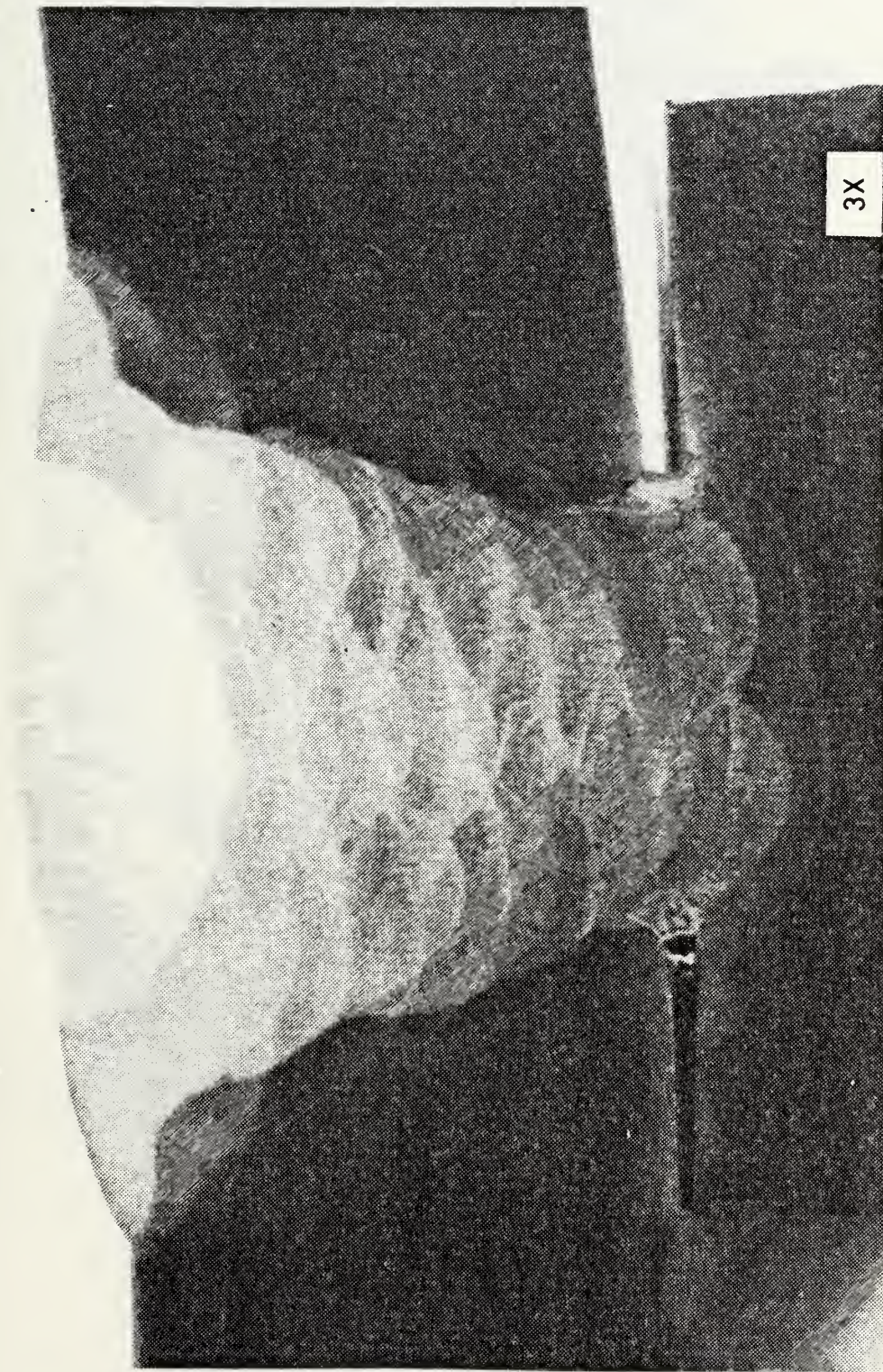


Figure 5 Photo of SAW Macroetched Specimen

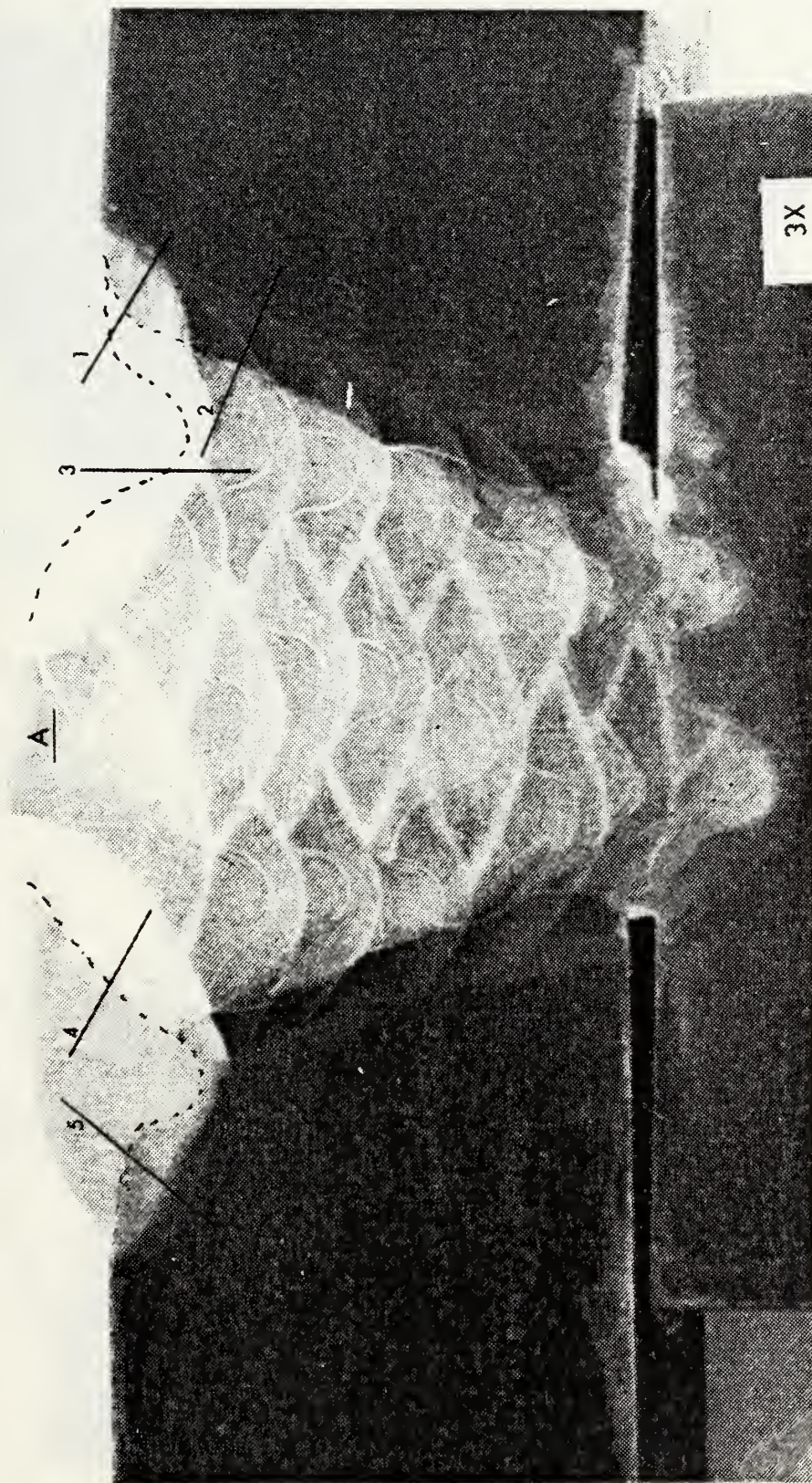


Figure 6 GMAW Microhardness Traverses Indicated to Scale (dotted lines indicates fusion lines)

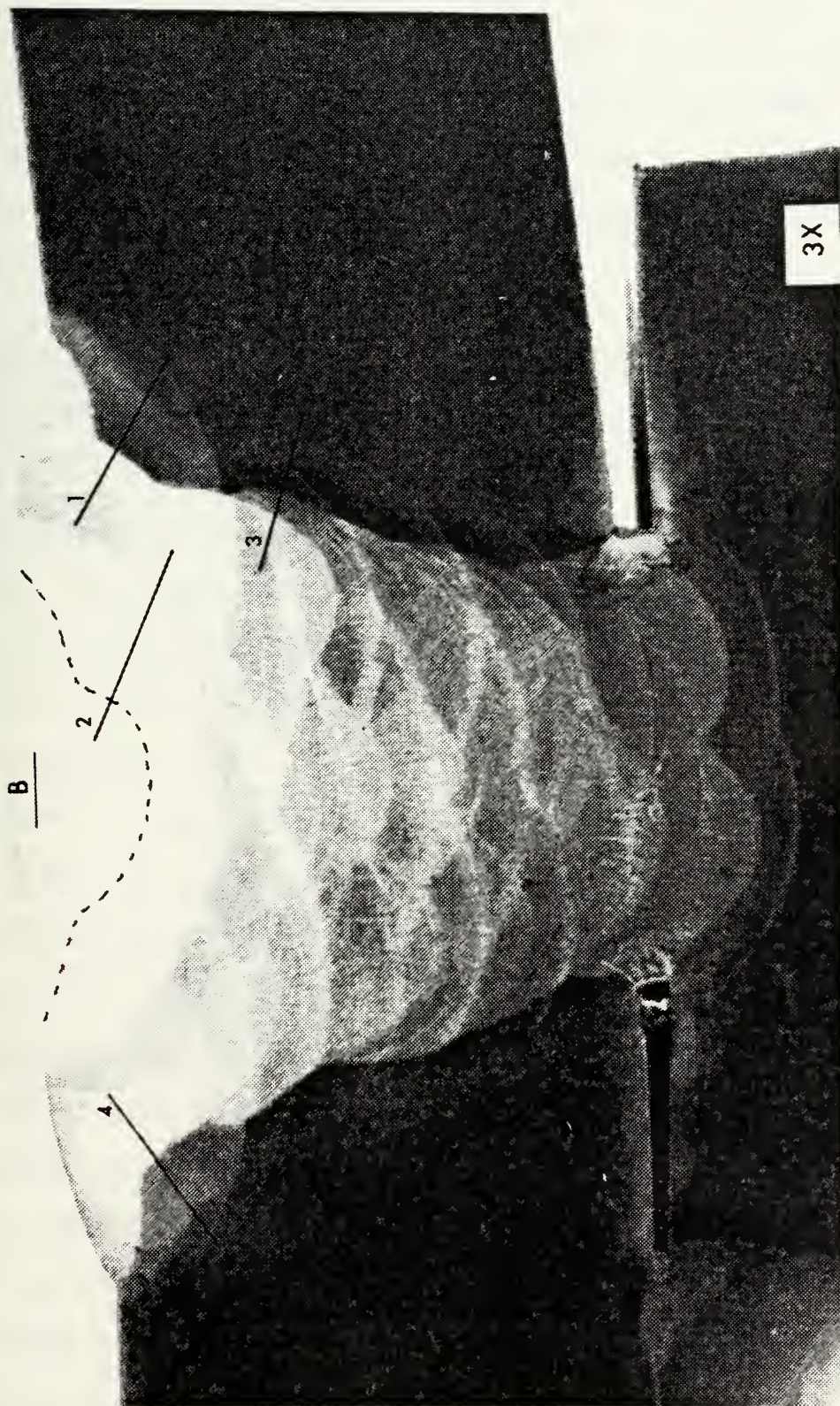


Figure 7 SAW Microhardness Traverses Indicated to Scale (dotted line indicates fusion line)

remove the etch and dark field microphotographs was taken in an attempt to characterize the distribution of micro-inclusions in the upper weld and coarse-grained HAZ. Inclusion counts on weld metals were made by counting the number of inclusions traversed in a known area at a magnification of 425x.

D. ELECTRON MICROSCOPY SAMPLE PREPARATION

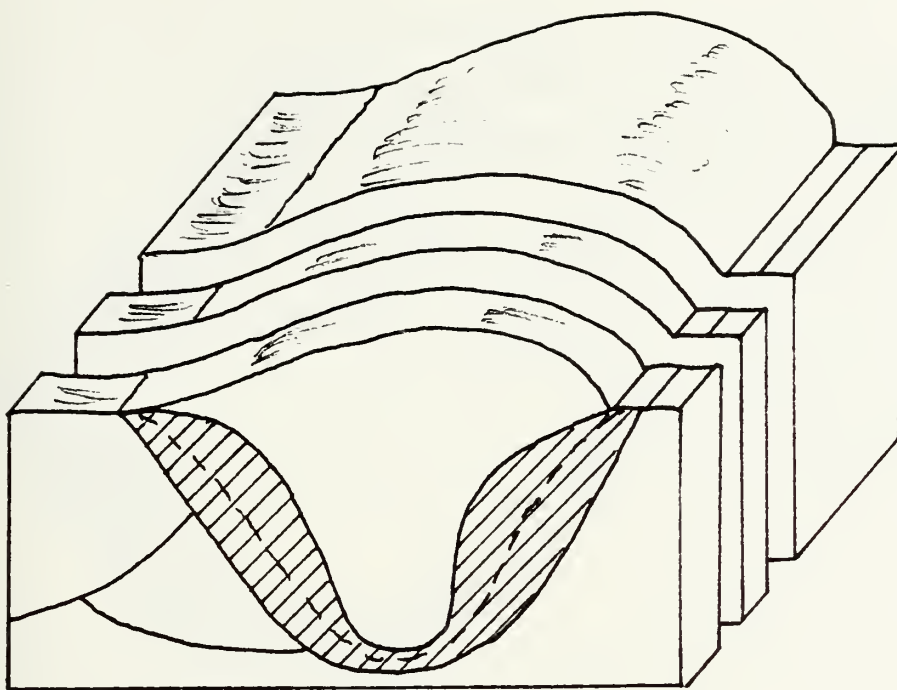
The last pass from each weldment was then wafered along a plane perpendicular to the plane of the weld using a low speed diamond wafering saw, Figure 8(a) and 9(a). A wafer from each weldment was then mounted on a flat steel block using the two sided adhesive tape for sanding and polishing using standard metallographic sample preparation techniques.

Each wafer was then etched in 2% Nital for 20 seconds and a line was scribed from the upper-weld region near the surface extending through the largest area of HAZ, which also contained the largest coarse-grained region in the HAZ. Scribed perpendicular to this line were lines indicating the fusion line and end of coarse-grained HAZ. The specimens were then mounted appropriately for scanning electron microscopy (SEM). In order to characterize the microstructure, photomicrographs were taken every 0.1 mm along the scribed portions of each weldment so that the upper-weld, fusion line, coarse-grained and fine-grained HAZ's could be characterized Figure 8(b) and 9(b).

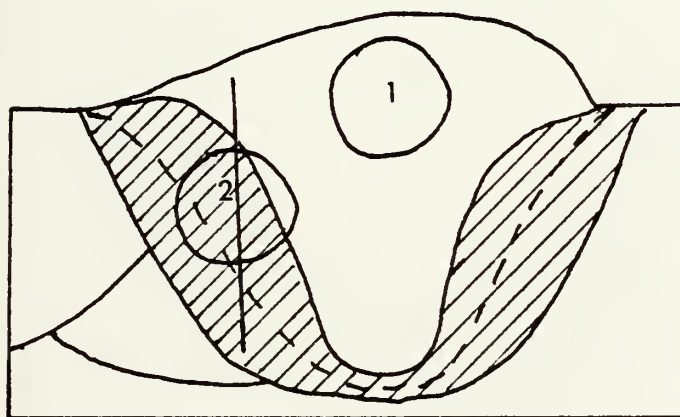
Wafers from each weldment were prepared for transmission electron microscopy (TEM). Each wafer was thinned from 150 microns to approximately 125 microns by hand sanding. Three-millimeter discs were punched-out from the upper-weld region and the coarse-grained HAZ as shown in Figure 8(b) and 9(b). These discs were electropolished using a 10% perchloric acid, 90% methanol electrolyte cooled to approximately -45°C. Electropolishing was performed with 16 volts and 50 milliamperes using a Tenupol twin jet thinning apparatus. Transmission electron microscopy was utilized to characterize and compare the microstructures of each weldments upper-weld and coarse grained HAZ. TEM was conducted using a JEM120CX microscope operating at 120 KeV.

E. NOTCHED BAR IMPACT TESTING

NSRDC prepared 30 charpy (Simple-Beam) impact test specimen from each weldment. All 60 specimens were etched in 2% Nital to reveal weld metal characteristic so that the center of the weld could be located and marked for machining of V-notch. Each specimen were machined to conform to ASTM standards. The specimens were fractured on a Tinius Olsen (264 ft-lb) Impact Tester, at temperatures ranging from 60°C to -196°C. At least 2 specimens were tested at each temperature and an average energy absorbed value was recorded. Standard ductile-to-brittle-transition temperature (DBTT) curves were developed for GMAW and SAW weldments.

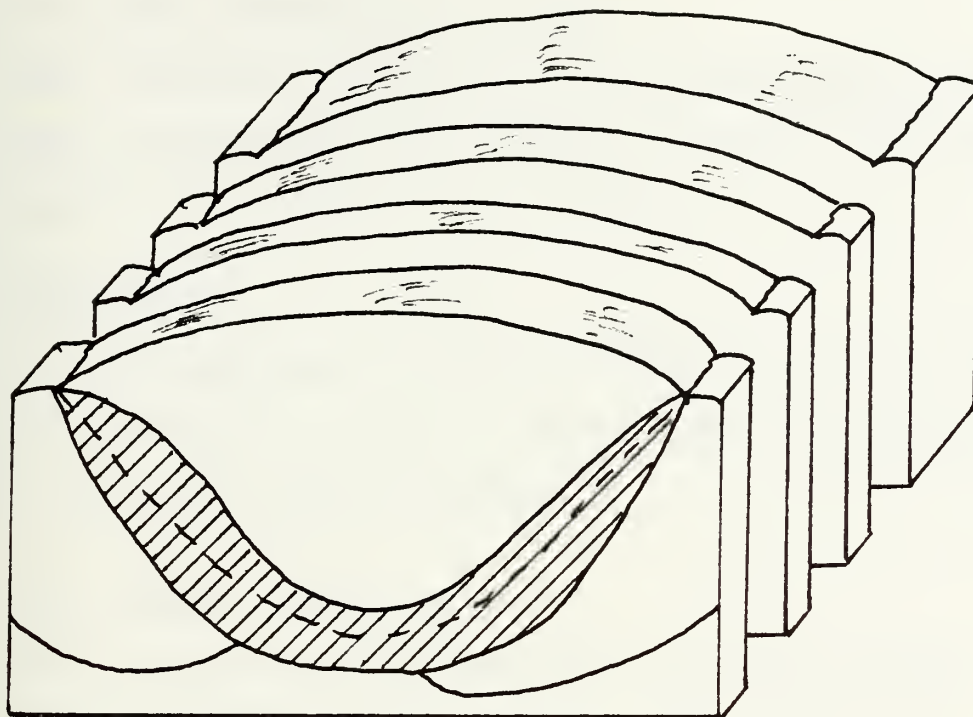


(a)

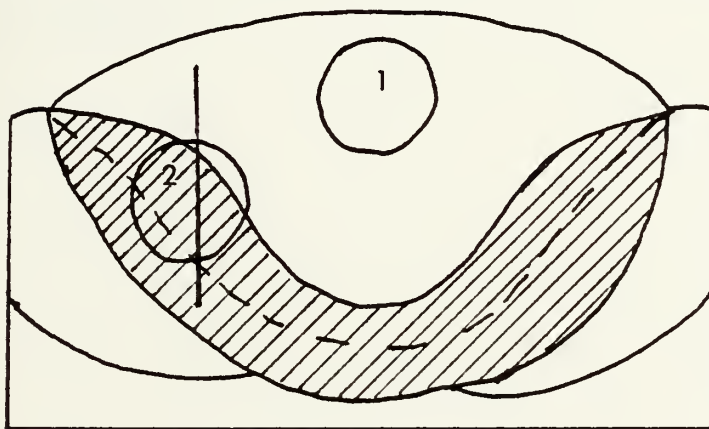


(b)

Fig. 8 Sectioned last pass in GMAW weldment showing:
 (a) wafer cutting technique and (b) 3 mm TEM foil
 locations in upper-weld region (1) and in coarse-
 grained HAZ (2), also scribed line used in SEM
 mapping.



(a)



(b)

Fig. 9 Sectioned last pass in SAW weldment showing:
 (a) wafer cutting technique and (b) 3 mm TEM foil
 locations in upper-weld region (1) and in coarse-
 grained HAZ (2), also scribed line used in SEM
 mapping.

F. WELD METAL CONSTITUENT ANALYSIS

NSRDC conducted a weld metal constituent analysis for the GMAW and SAW weldments, through a private laboratory and provided the results to the author.

G. FRACTOGRAPHY

Fractured surfaces from fully ductile and fully brittle charpy specimens were mounted appropriately for observation in the scanning electron microscope.

H. WELD PROCESS COOLING RATES

NSRDC measured the cooling rates for each weldment and provided the results to the author. The thermocouple plunge technique was used to measure cooling rates (see Figures 2 and 3).

IV. EXPERIMENTAL RESULTS

A. MECHANICAL PROPERTIES

1. Microhardness Testing

The Vickers microhardness traverses for each specimen were plotted and the results are illustrated in Figures 10 and 11. For ease of discussion and comparison of results between both weldments, five separate regions have been selected and are illustrated in each figure as listed below.

Region A: Weld Metal

Region B: Coarse Grained HAZ

Region C: Fine Grained HAZ

Region D: Tempered Weld Metal from Previous Pass

Region E: Parent Base Metal

2. Hardness Profiles for GMAW

Traverse A-1 Figure 10(a) was taken from the last pass (pass #20 Figure 2) and is therefore untempered by subsequent passes. The hardness profile indicates that weld metal hardness is relatively constant at 300 HV.

Measurements crossing into the HAZ revealed a significant jump in Vickers hardness reaching a peak value of 430 HV in the coarse-grained HAZ and declining steadily through the fine-grained HAZ until reaching a steady value of 230 HV in the parent base metal. Traverse A-5 Figure 10(b)

(pass #19 Figure 2) is also an untempered pass and its hardness profile is almost identical to that of A-1 except that the weld metal hardness in A-5 is 330 HV, which is 30 HV more than the weld metal in A-1. This can be explained by carefully observing Figure 6. It can be seen that a greater amount of base plate metal was melted by pass #19 (A-5) than in pass #20 (A-1). Therefore, increased weld metal dilution and thus a higher hardenability weld metal would account for the increases in hardness of the weld metal in traverse A-5. Conversely, a reduction in weld metal hardness in traverse A-4 Figure 10(c) as the traverse proceeds into weld pass #17 approximately 3 to 4 millimeters from the fusion line (Region D).

Traverse A-2 Figure 10(d) was made in order to measure the effect on hardness when crossing two separate HAZ's. The first 2 millimeters (-5 mm to -3 mm) of region A is HAZ from pass #20 and this accounts for the 340 HV value obtained, and correlates well with the hardness obtained for the HAZ of traverse A-3, Figure 10(c). The region from -2.4 mm to 0 mm in A-2 is at 250 HV and represents tempered weld metal from pass #14. The base metal HAZ that follows after crossing the visible fusion line is represented by a two-tier plateau. The first plateau which is the base metal HAZ from pass #14 peaks at 400 HV, then drops to the next plateau which is the HAZ from pass #12 (tempered by pass #14) which stays constant at 300 HV, then falls off to

HY-100 GMAW

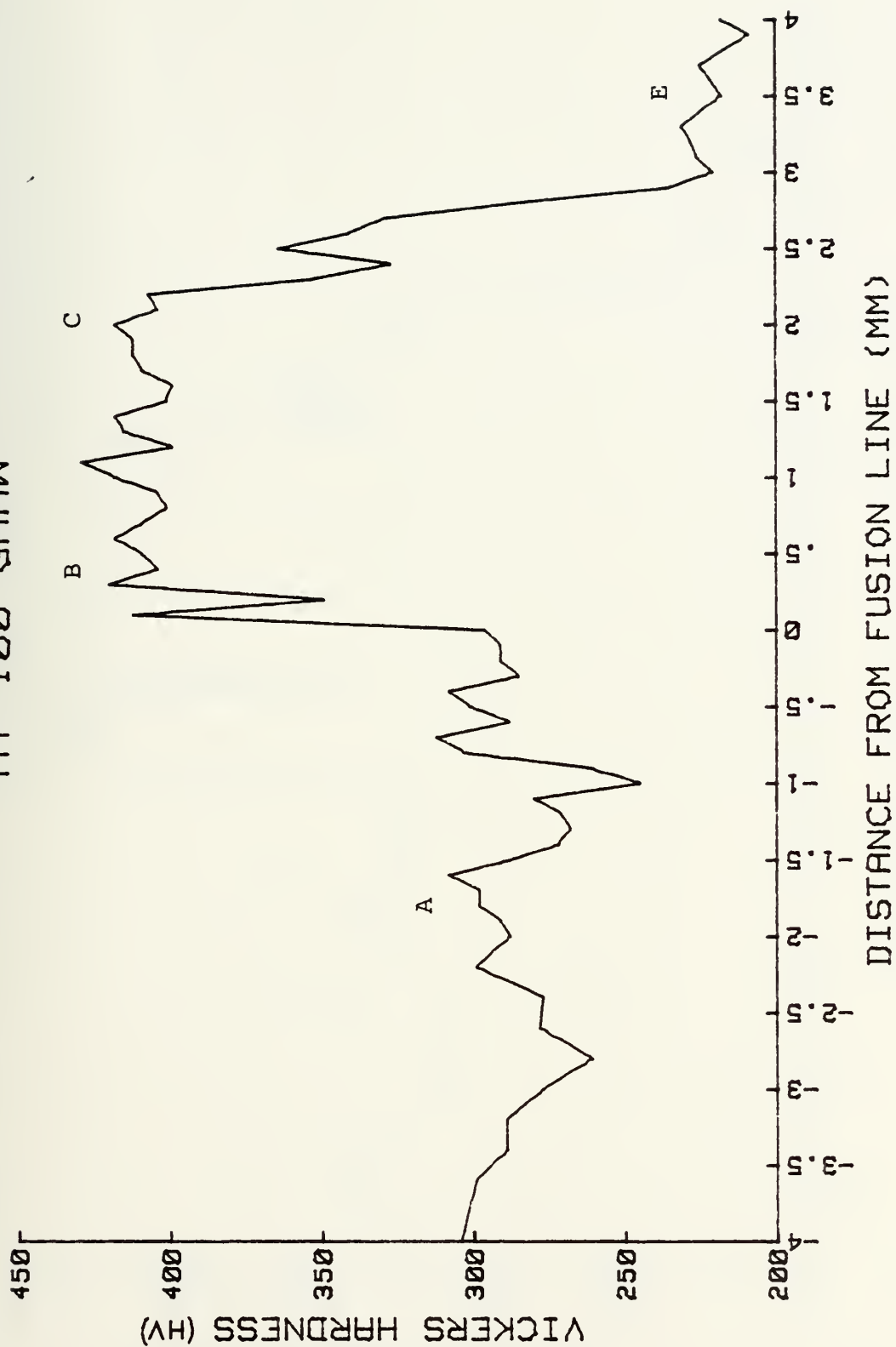


Figure 10(a) Vickers Hardness Traverse A-1 (GMAW)

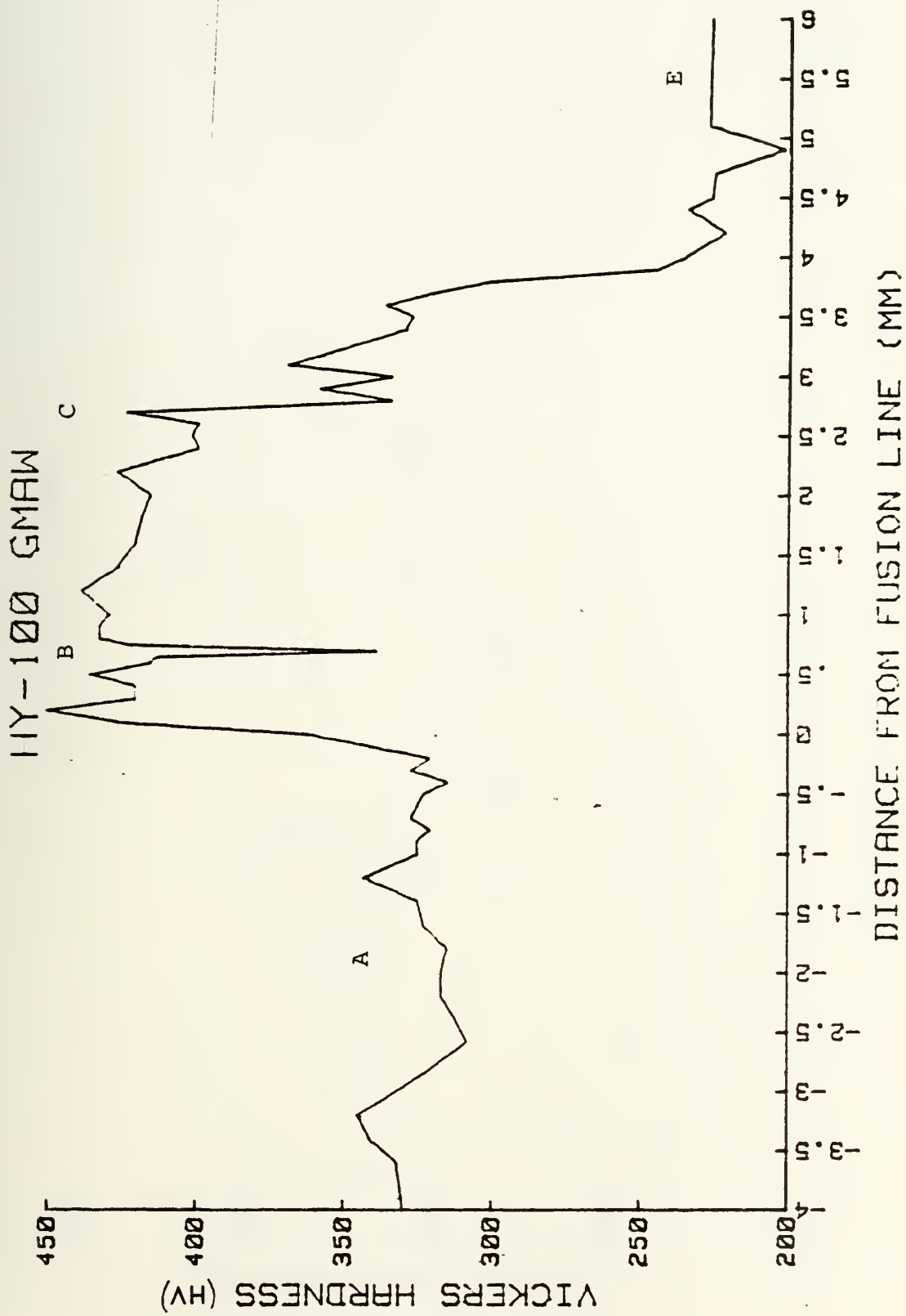


Figure 10(b) Vickers Hardness Traverse A-5 (GMAW)

HY-100 GMAW

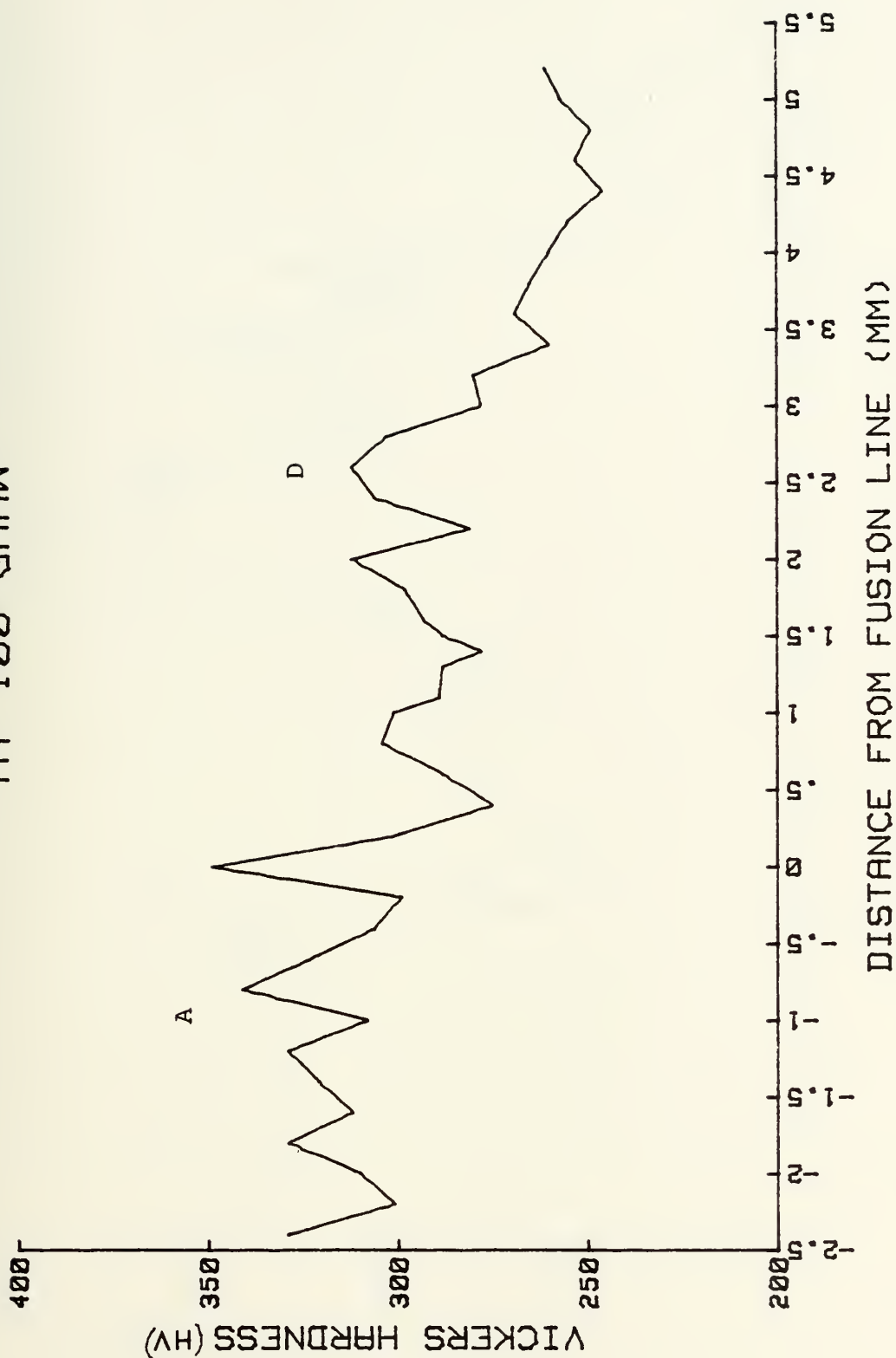


Figure 10(c) Vickers Hardness Traverse A-4 (GMAW)

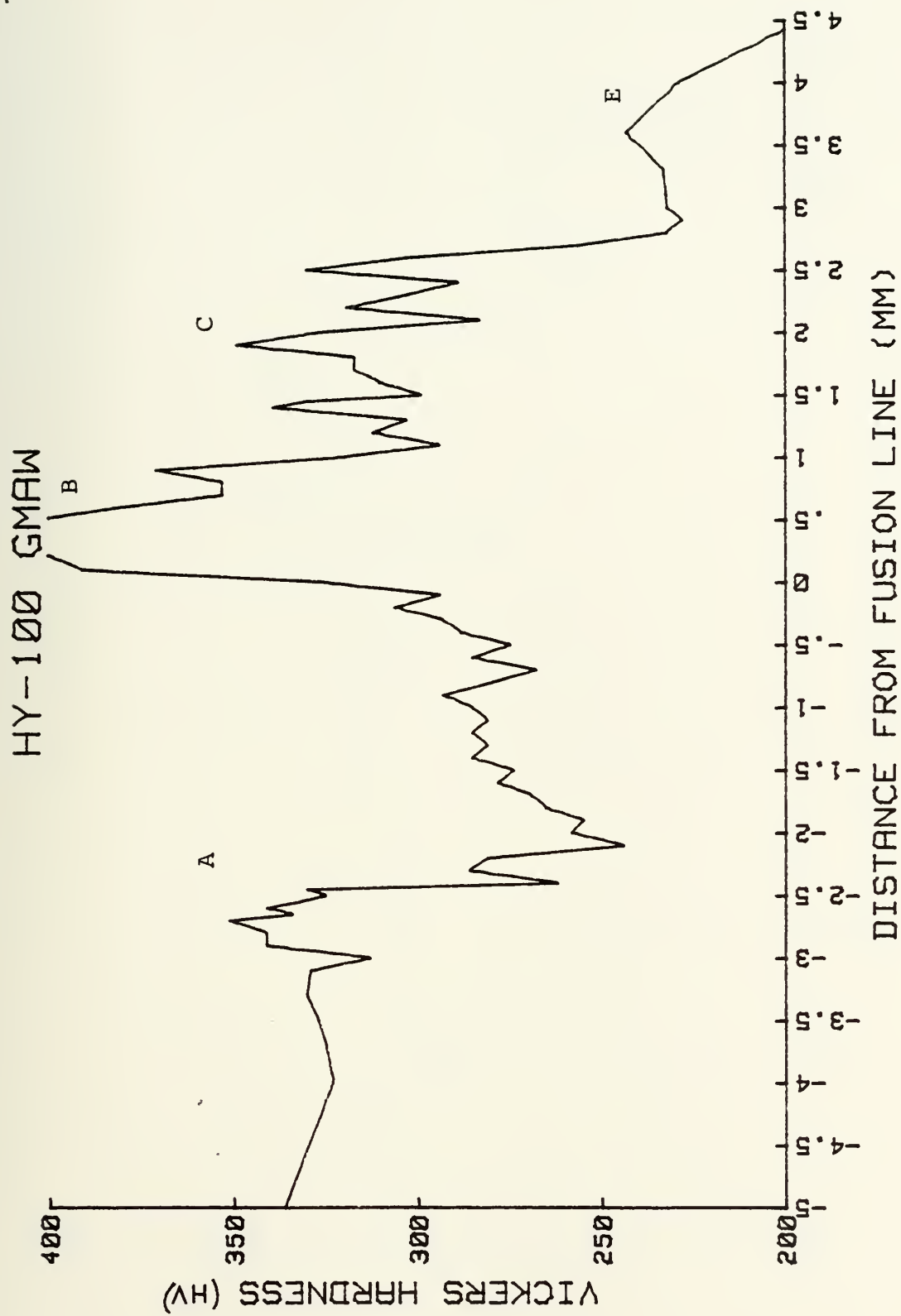


Figure 10(d) Vickers Hardness Traverse A-2 (GMAW)

HY-100 GMAW

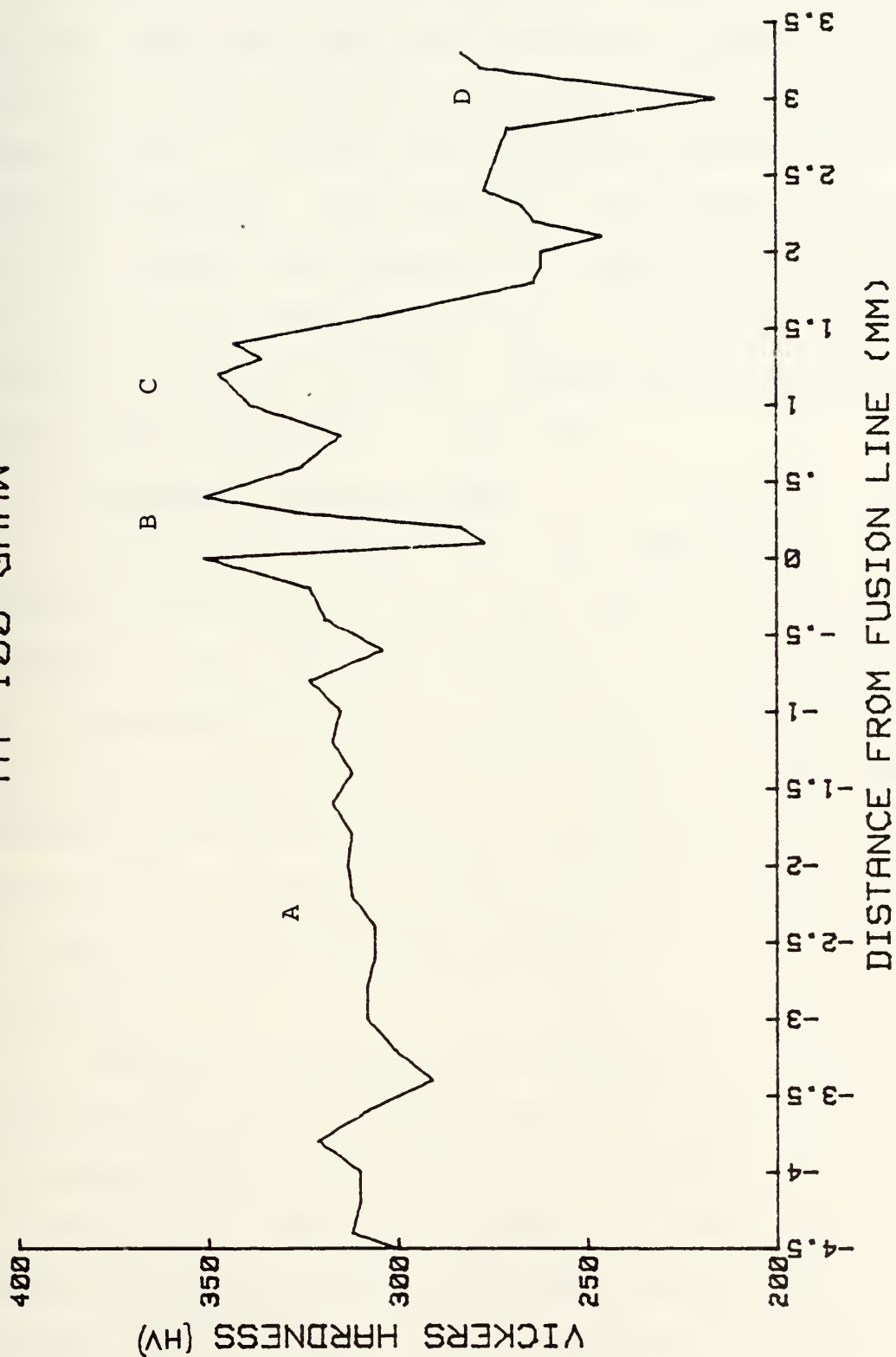


Figure 10(e) Vickers Hardness Traverse A-3 (GMAW)

230 HV which is the parent case metal. Traverse A-3 Figure 10(e) was taken well away from the effects of base metal dilution in order to more closely approximate a similar traverse taken in the last pass of the SAW weldment for comparison purposes. As can be seen, hardness measurements vary only slightly when crossing the fusion line of pass #20 into its HAZ. The hardness then drops from a peak hardness of 330 HV in the HAZ to approximately 250 HV in the tempered weld metal of pass #14.

3. Hardness Profiles for SAW

Traverse B-1, Figure 11(a) was taken in pass #18 in a region unaffected by the last pass (#20) as can be seen in Figure 7. The weld metal hardness is constant at 260 HV and as measurements cross the visible fusion line hardness jumps significantly from 260 HV to a peak of 400 HV. The hardness then declines gradually as measurements show the effect of first, crossing the HAZ's for both passes #15 and #18, until reaching a Vickers hardness of 230 HV in parent base metal.

Excellent agreement with hardnesses in Traverse B-1 is seen in Traverse B-4 Figure 11(b), taken in pass #19 in a region unaffected by the last pass (#20). Traverse B-3, Figure 11(c) was taken in pass #15 so that effects on hardness across HAZ's for two different passes could be observed, similar to that taken in Traverse A-2 (GMAW). The weld metal hardness remains constant at 260 HV from -4

HY-100 SAW

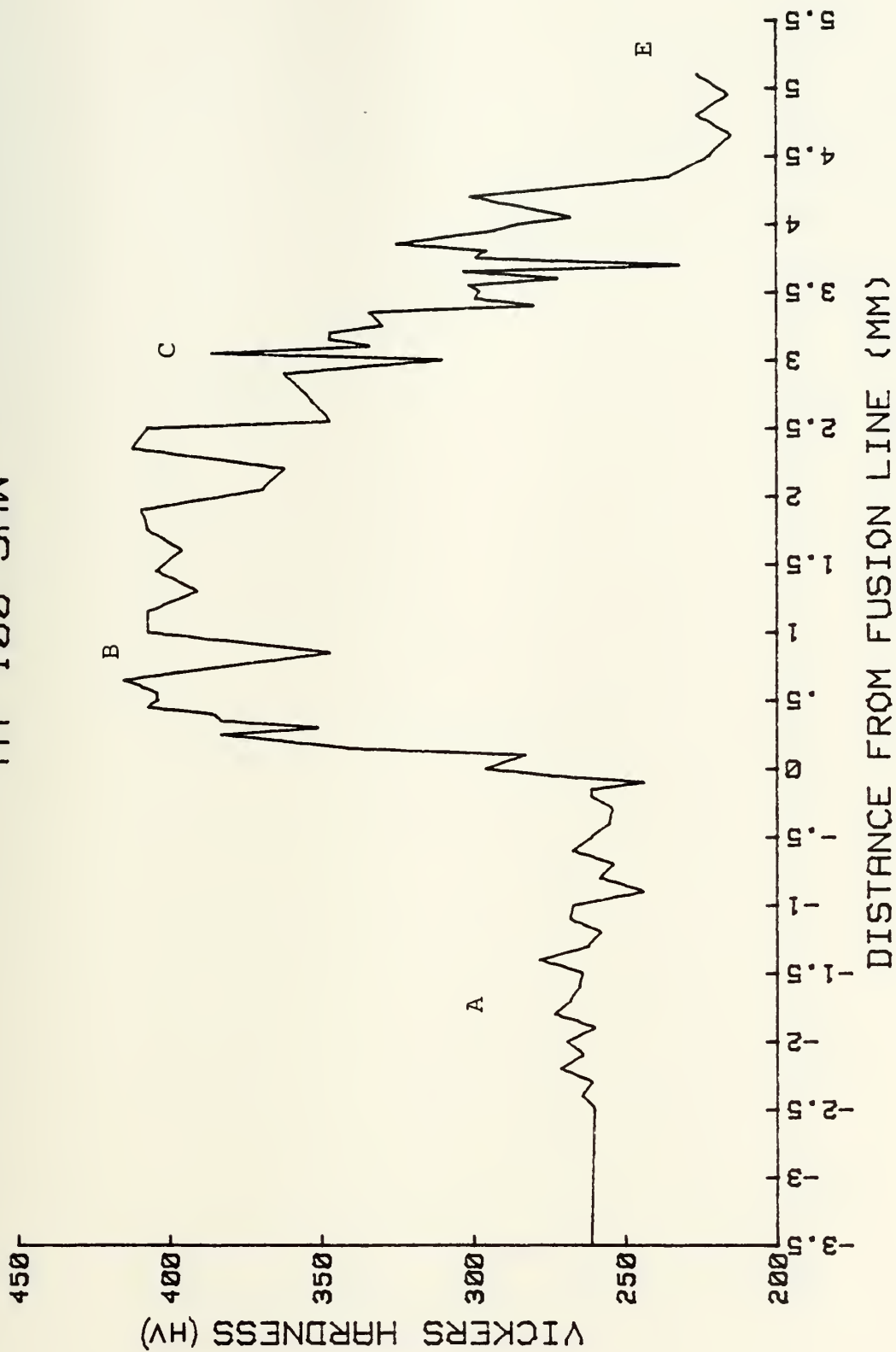


Figure 11(a) Vickers Hardness Traverse B-1 (SAW)

HY-100 SAW

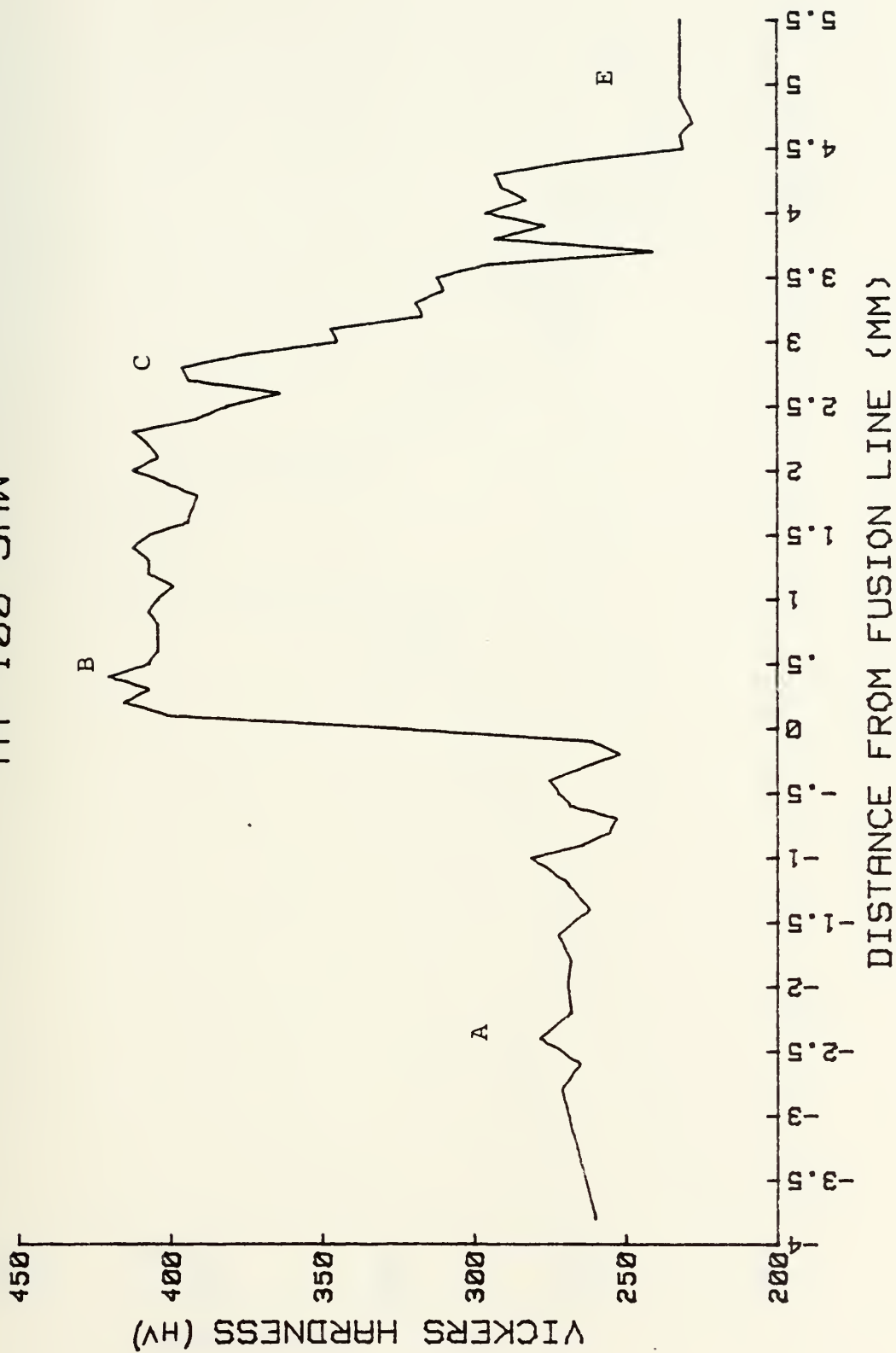


Figure 11(b) Vickers Hardness Traverse B-4 (SAW)

HY-100 SAW

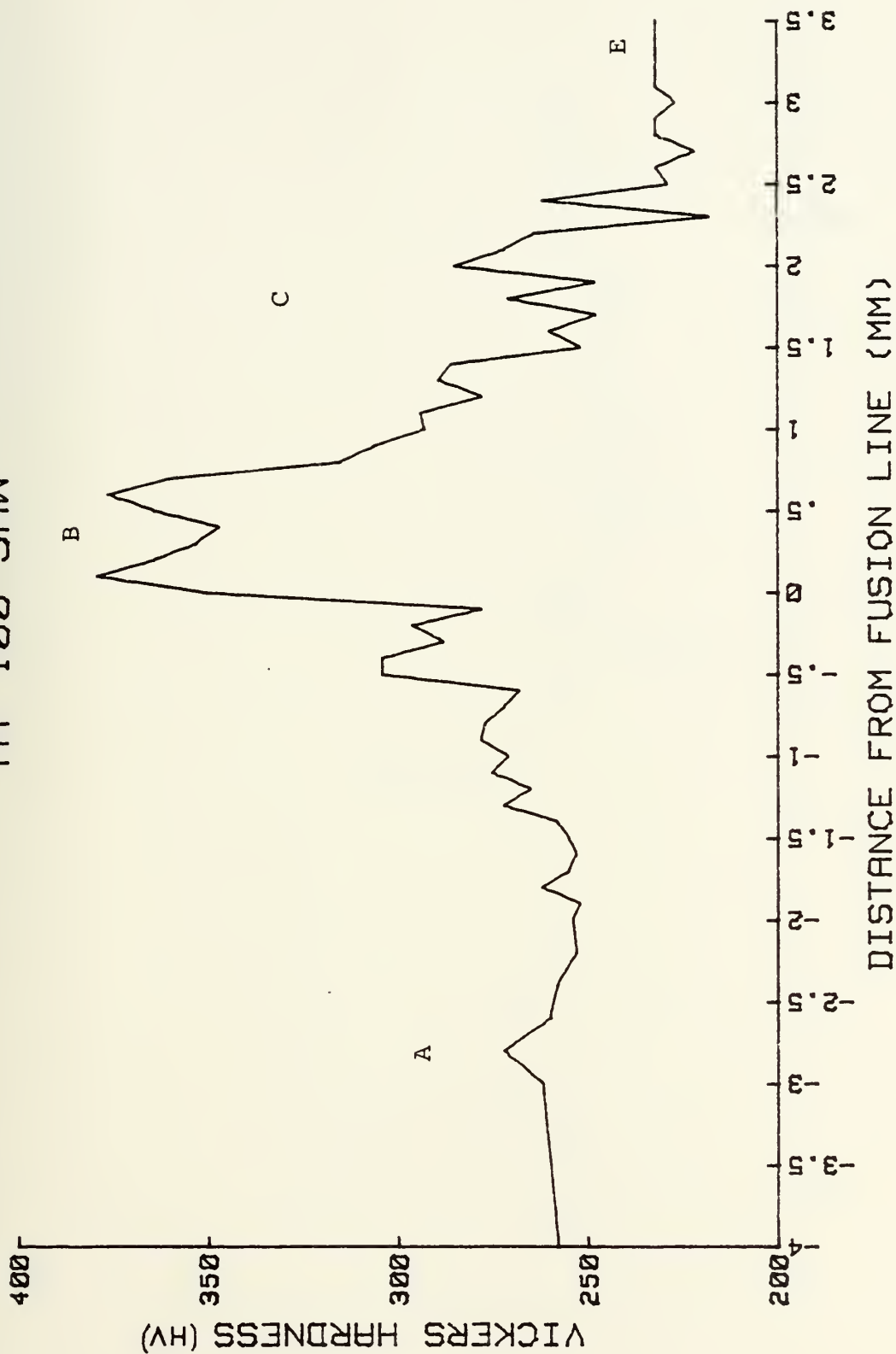


Figure 11(c) Vickers Hardness Traverse B-3 (SAW)

HY-100 SAW

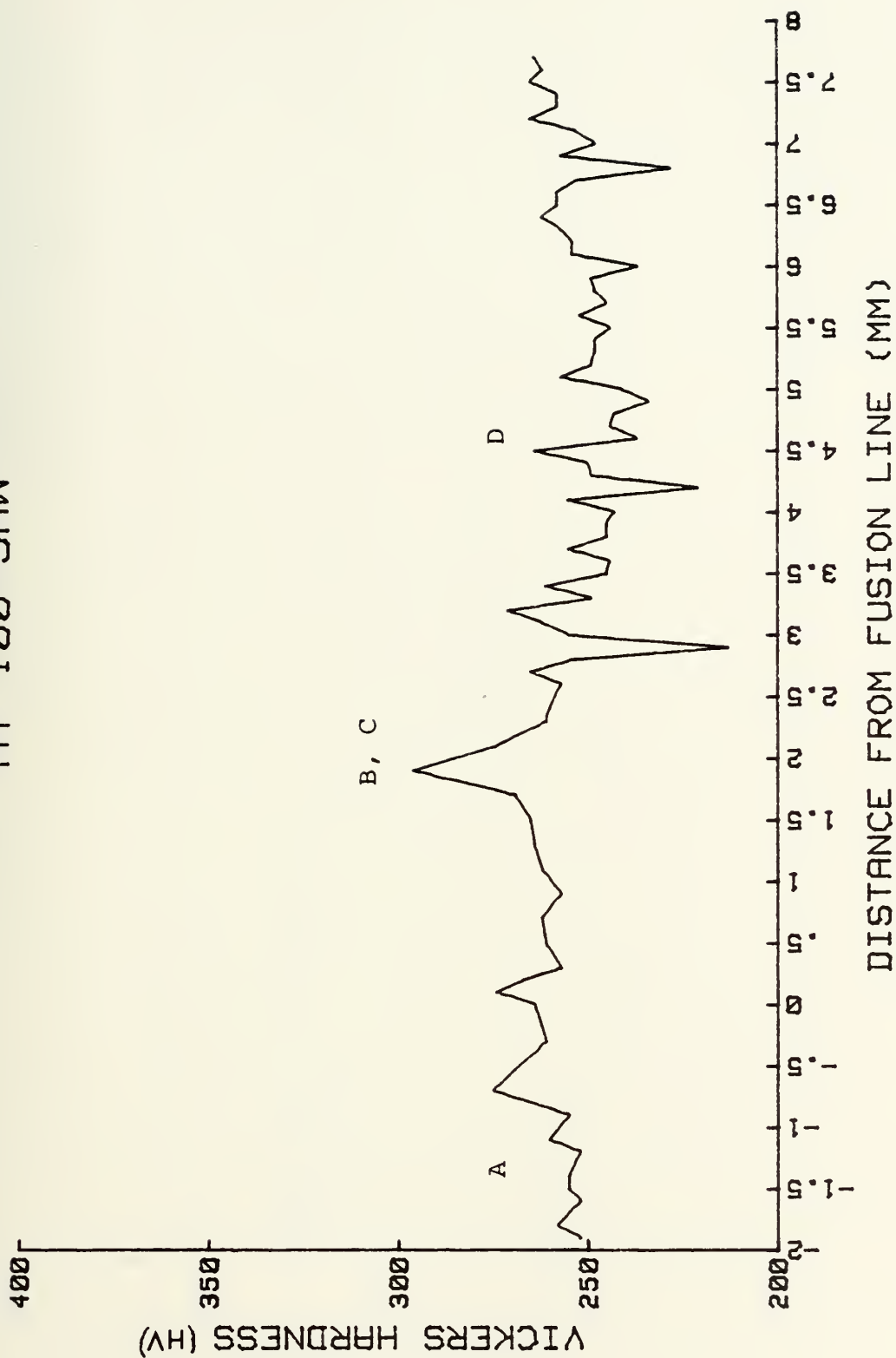


Figure 11(d) Vickers Hardness Traverse B-2 (SAW)

HY-100 GMAW & SAW

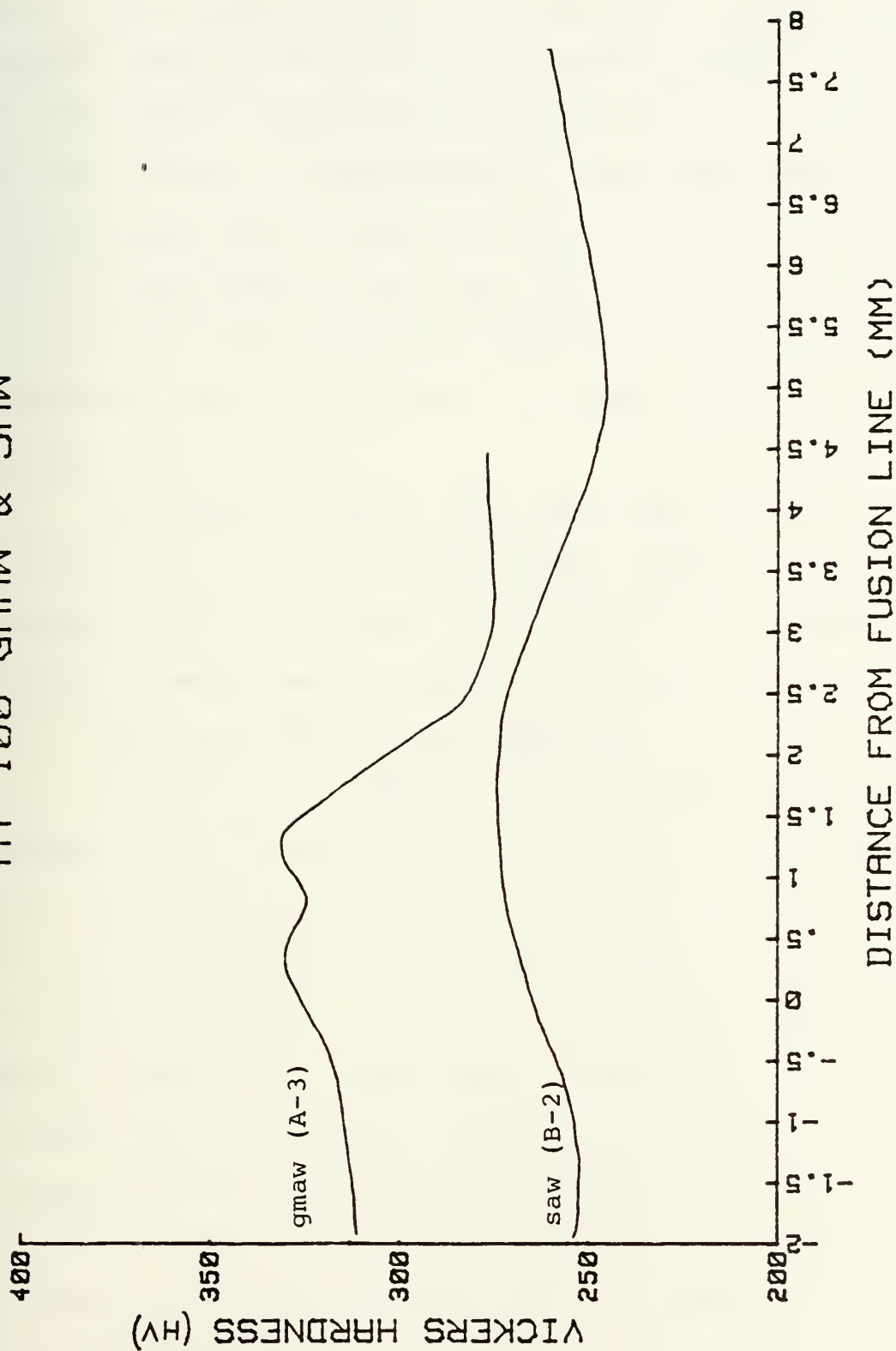


Figure 12 Vickers Hardness Traverses A-3 and B-2

mm to -1 mm. From this point to the visible fusion line, hardness jumps to 300 HV as the traverse crosses into pass #15's HAZ which is weld metal from pass #12. The base metal HAZ that follows is represented by a two-tier plateau. The first plateau which is base metal HAZ from pass #15 peaks at 380 HV then drops to the next plateau between 1 mm and 2.5 mm which is the base metal HAZ resulting from pass #12 (tempered by pass #15). Parent base metal hardness is 230 HV.

Traverse B-2 Figure 11(d) was taken in the last pass (#20) and as can be seen hardness remains relatively constant at 250 HV throughout the traverse, increasing only slightly as measurements crossed the fusion line.

4. GMAW and SAW Hardness Comparison

Traverses A-3 (GMAW) and B-2 (SAW) were plotted together and are shown in Figure 12. Traverse A-3 begins in the weld metal of pass #20 (310 HV) and crosses the fusion line into the HAZ (330 HV) and then crosses into weld metal from pass #14 (260 HV). The lower hardness of the weld metal in pass #14 indicates some softening due to tempering from pass #20 has occurred. However in traverse B-2 where a traverse was made from pass #20 weld metal (260 HV) through the HAZ (270 HV) and crossing into pass #18 weld metal (250 HV) it is clear that pass #20 is not significantly reducing the hardness of pass #18.

5. Charpy Impact Test

From the data collected, curves were developed for the GMAW and SAW weldments and are shown in Figure 13 and 14 respectively. Based on the midpoint of the curve between the upper shelf and lower shelf, a DBTT of -70°C was assigned to the GMAW weldment and -20°C to the SAW weldment. For ease of comparison, the two curves are plotted together in Figure 15.

B. MICROSTRUCTURAL OBSERVATIONS

1. Light Field Optical Microscopy

Optical micrographs of GMAW and SAW weldments in the last pass are compared in Figure 16. It is very difficult to deduce any useful information from these photos since there appears to be no significant differences in microstructure between weldments and also within each weldment from the upper weld region to the coarse grained HAZ.

2. Dark Field Optical and TEM Microscopy

Micrographs were taken in order to study the general nature of the inclusion distribution in each weldment. In the GMAW weldment, the distribution is shown in Figure 17. In the SAW weldment, the distribution is shown in Figure 18. In general, there appears to be a greater population of inclusions in the SAW weldment than in the GMAW weldment. The largest inclusions visible at the TEM level in Figures 17(c) and 18(c) are approximately 0.5 microns in diameter. The smallest inclusions visible at the

HY-100 WELDMENT DBTT CURVE GMAW

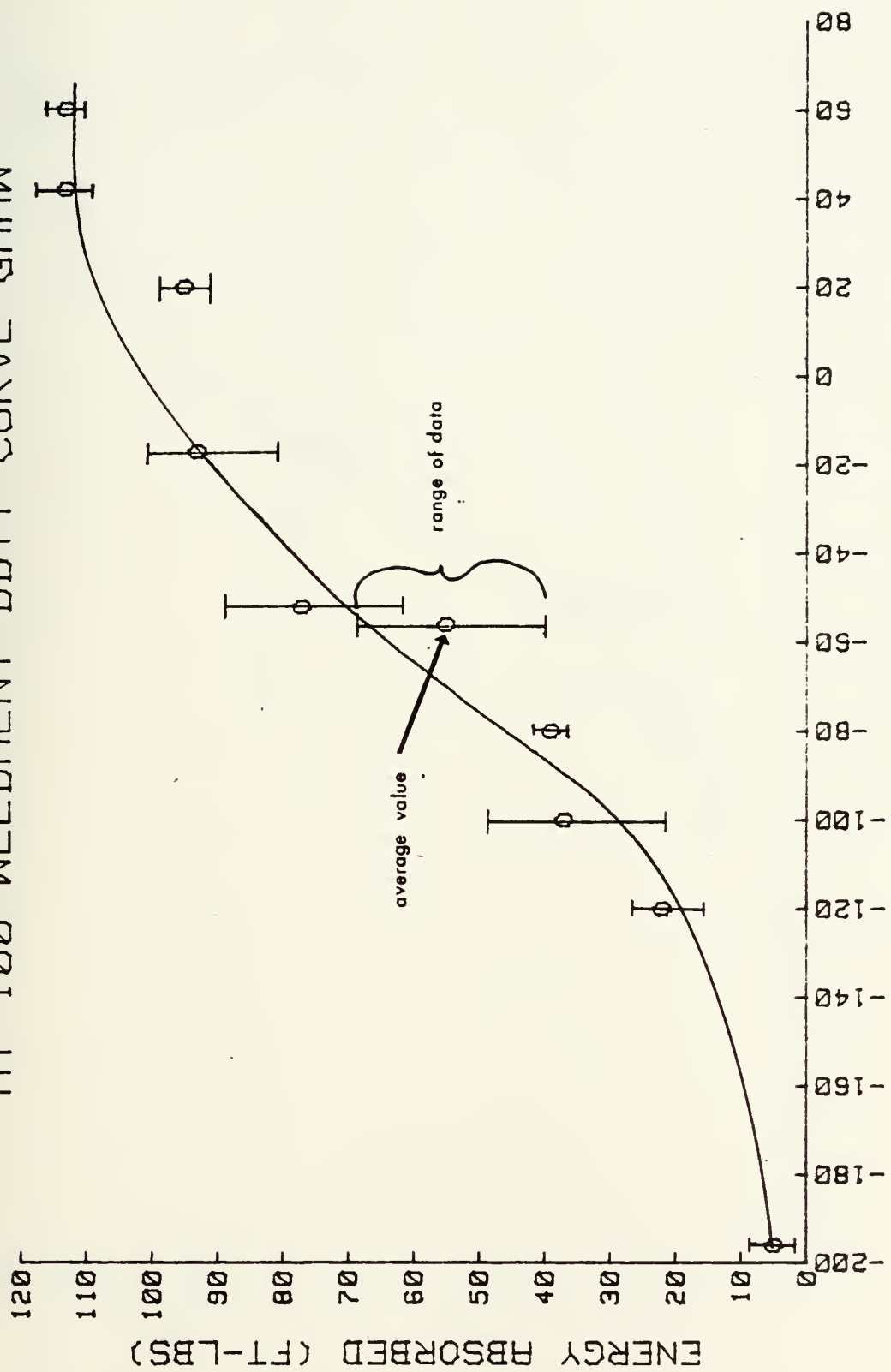


Figure 13 Ductile-to-brittle transition temperature (DBTT) curve for GMAW weldment

HY-100 WELDMENT DBTT CURVE SAW

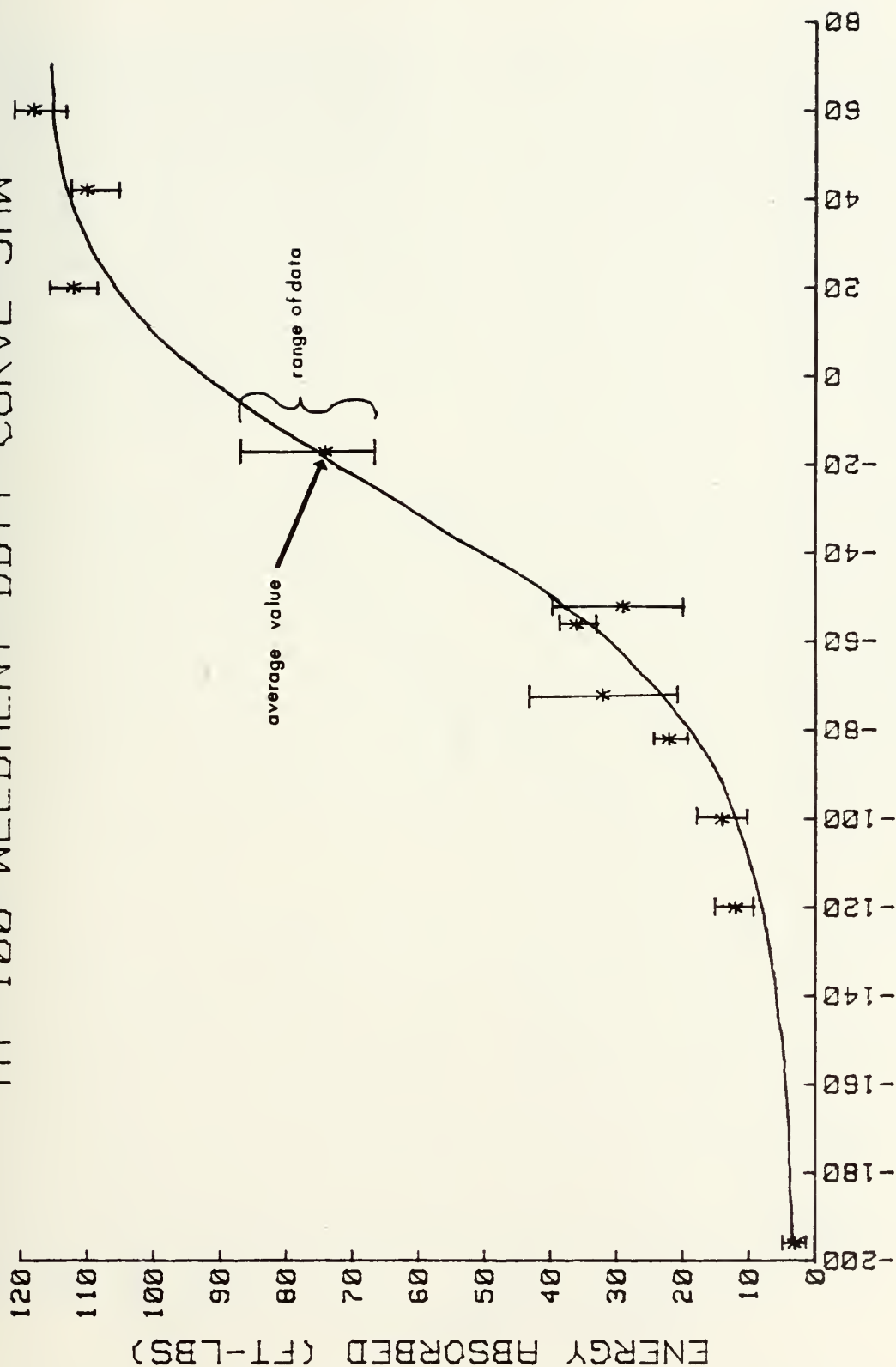


Figure 14 Ductile-to-brittle transition temperature (DBTT) curve for SAW weldment

HY-100 DBTT CURVES SAW & GMAW

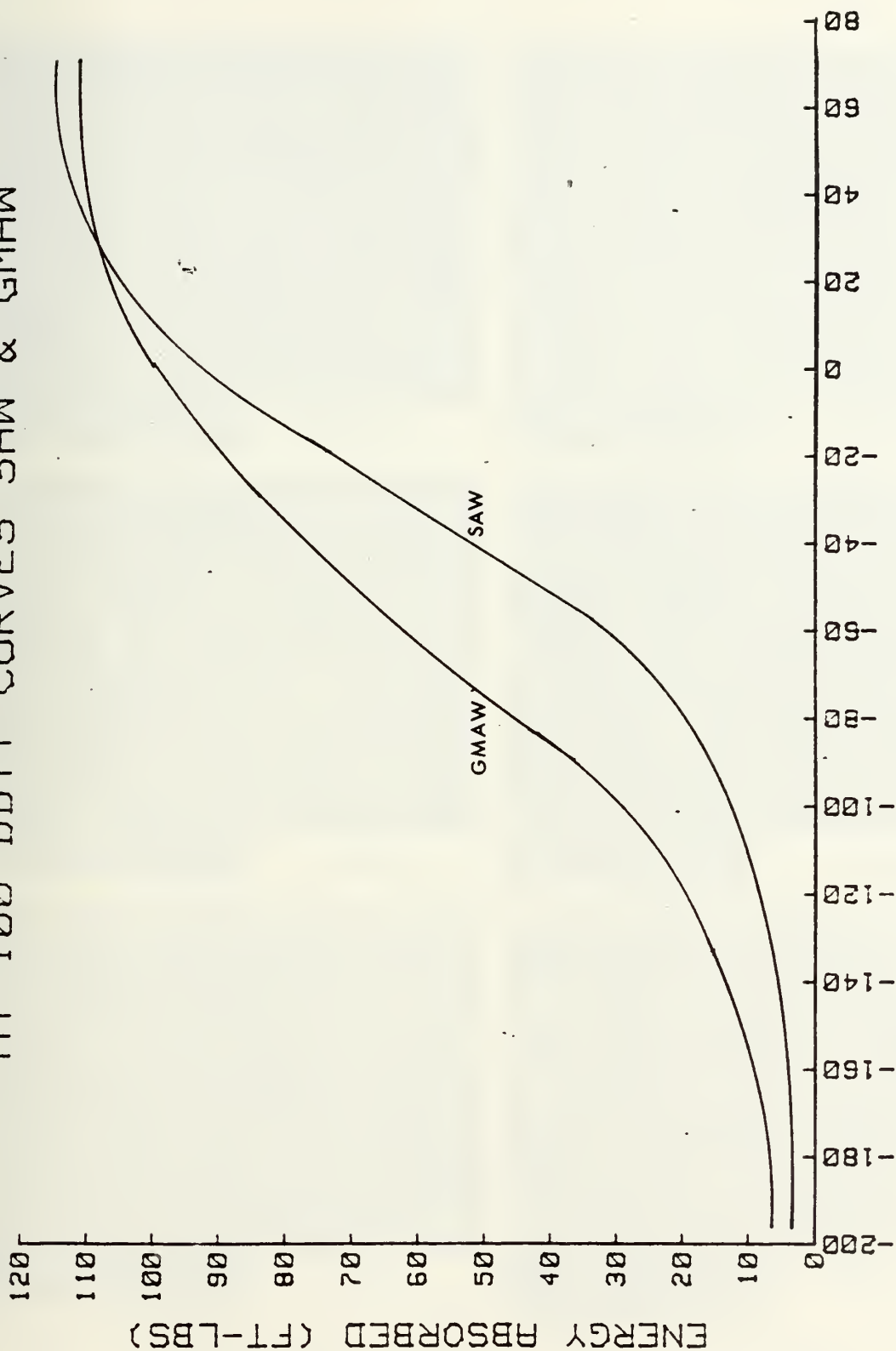


Figure 15 Ductile-to-brittle transition temperature curves for GMAW and SAW weldments

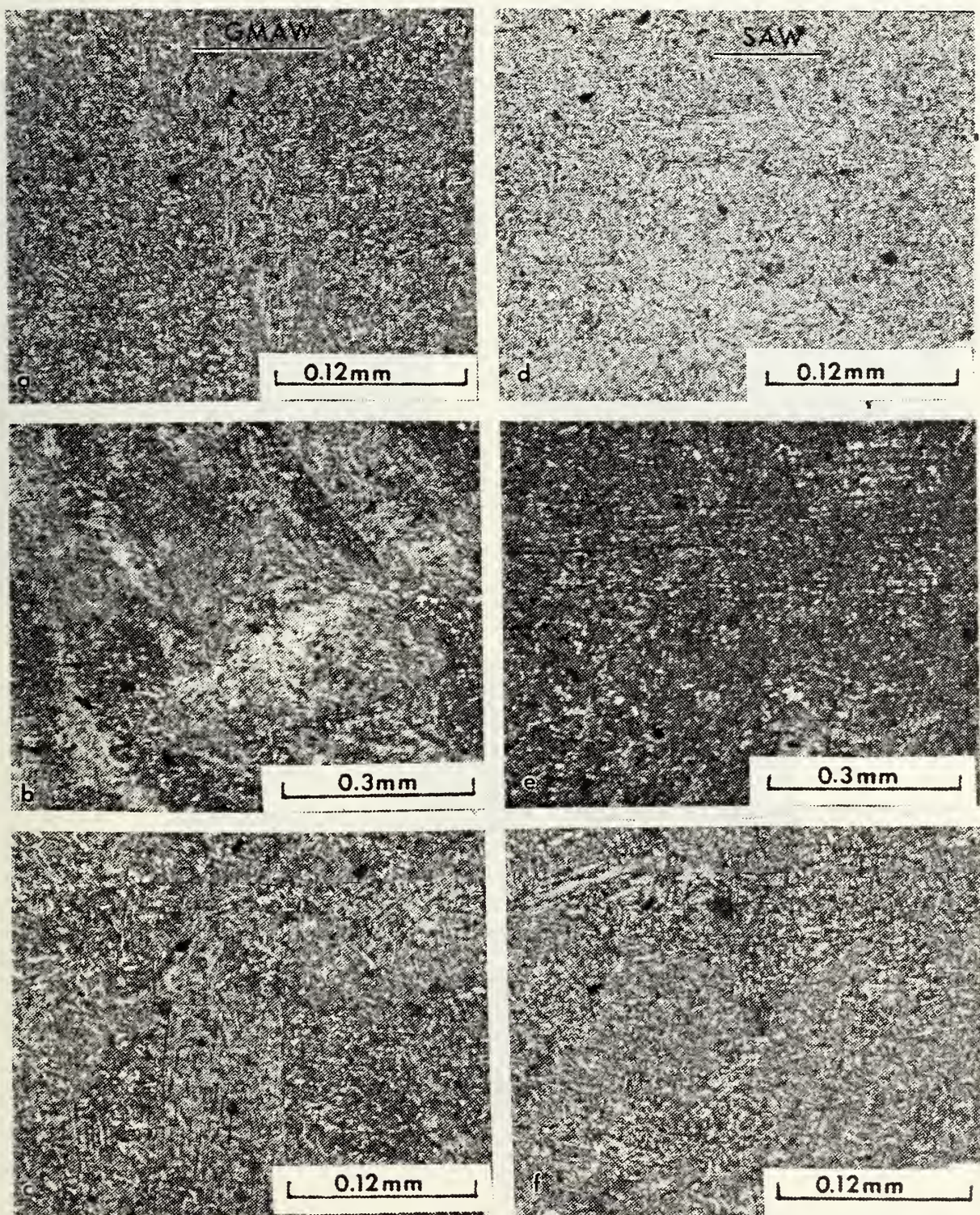


Figure 16 Optical micrographs of GMAW and SAW weldments in last passes showing: (a and d) upper-weld region (b and e) fusion line and (e and f) coarse-grained HAZ.

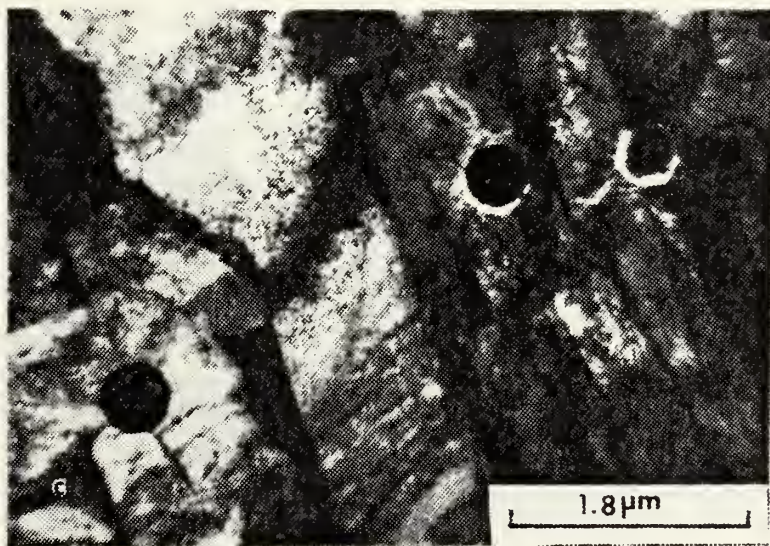
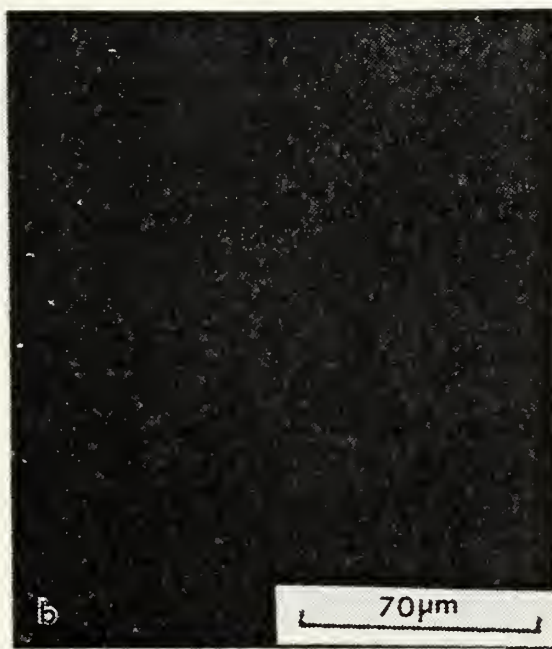
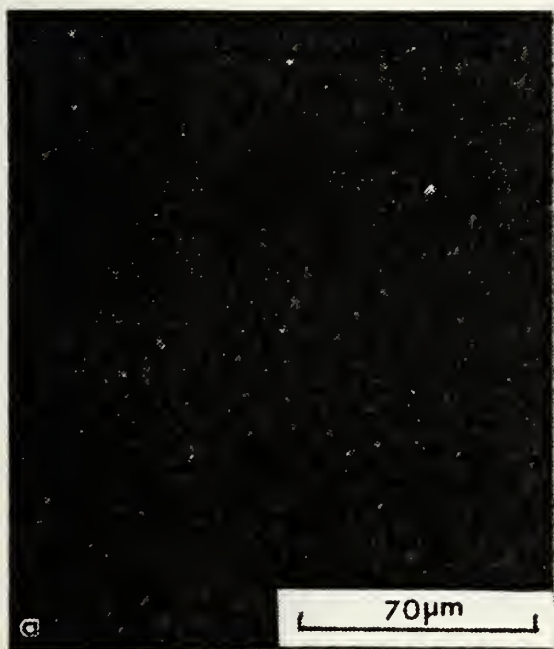


Figure 17 Optical dark field and TEM micrographs of GMAW weldment showing typical inclusion distribution in (a) upper-weld region, (b) coarse-grained HAZ and (c) upper-weld region (TEM).

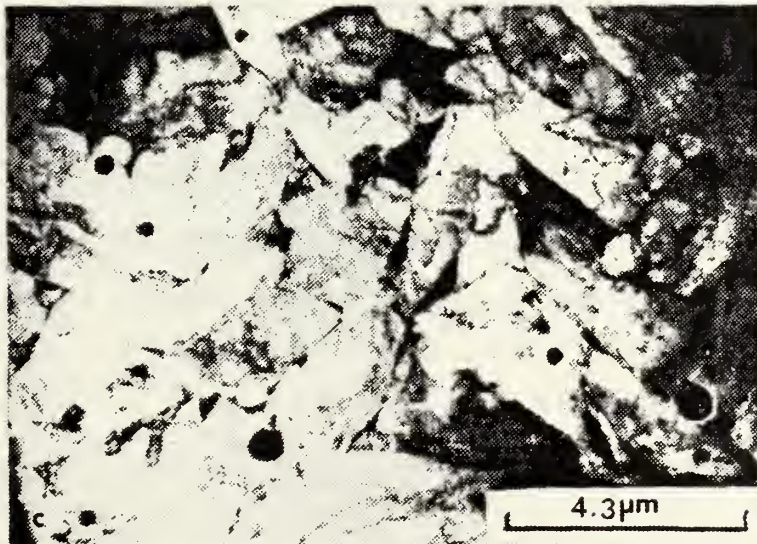
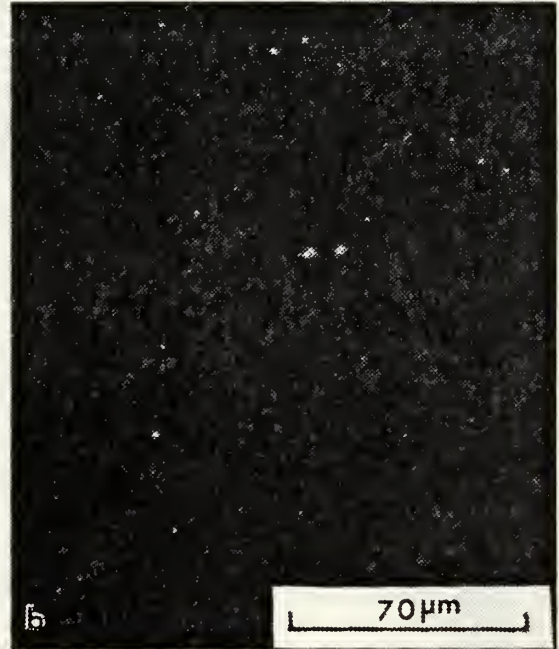
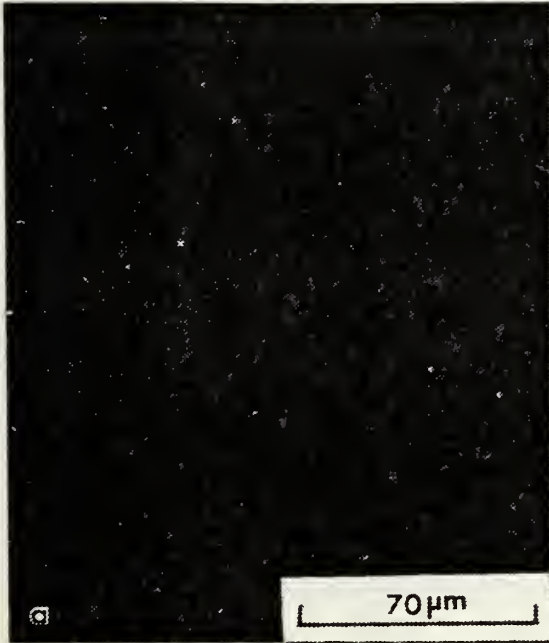


Figure 18 Optical dark field and TEM micrographs of SAW weldment showing typical inclusion distribution in (a) upper-weld region, (b) coarse-grained HAZ and (c) upper-weld region (TEM).

optical level Figures 17(a) and 18(a) are approximately 0.7 microns in diameter. These are believed to be the same type of inclusions. Micrographs in Figures 17(a) and 17(c), 18(a) and 18(c) were taken from the upper weld region. From these micrographs, a distribution of approximately 7,170 inclusions per square millimeter was calculated for the GMAW weldment and 9,550 inclusions per square millimeter for the SAW weldment.

3. Scanning Electron Microscopy

A micrograph of HY-100 base metal is shown in Figure 19. It represents a combination of tempered bainite and tempered martensite. Figure 20 is a comparison of the microstructures formed in the upper weld region, at the fusion line, weld metal coarse grained HAZ and fine grained HAZ for each weldment. Qualitatively it can be seen that the GMAW weldment consistently has a finer microstructure than its counterpart in the SAW weldment. Table 4 below illustrates the calculated average packet width in the upper weld region and in the coarse grained HAZ for each weldment.

Table 4

Average Packet Widths in GMAW and SAW Weldments

Region	GMAW Packet Widths (microns)	SAW Packet Widths (microns)
Upper Weld	1	2.6
Coarse Grained HAZ	2.4	3.2
Fine Grained HAZ	0.8	1.7

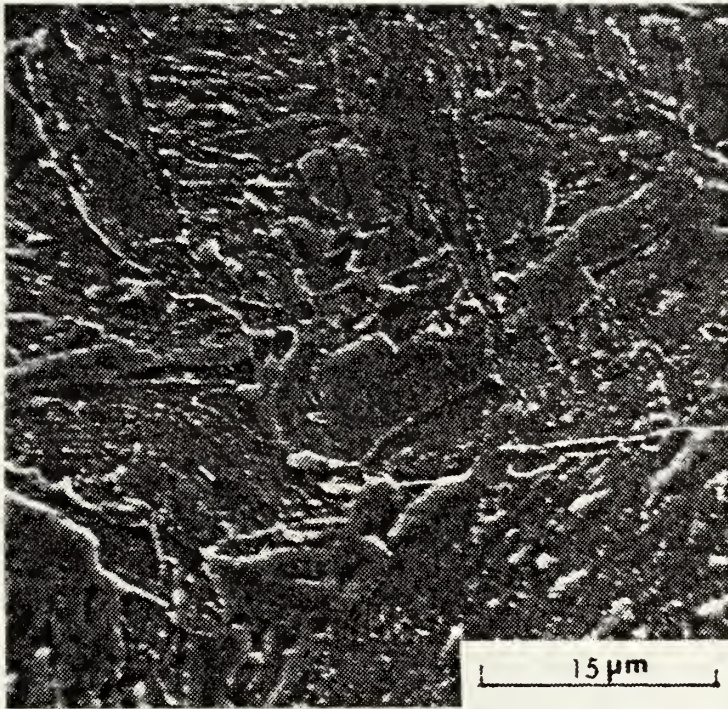


Figure 19 SEM Micrograph of HY-100 Base Metal

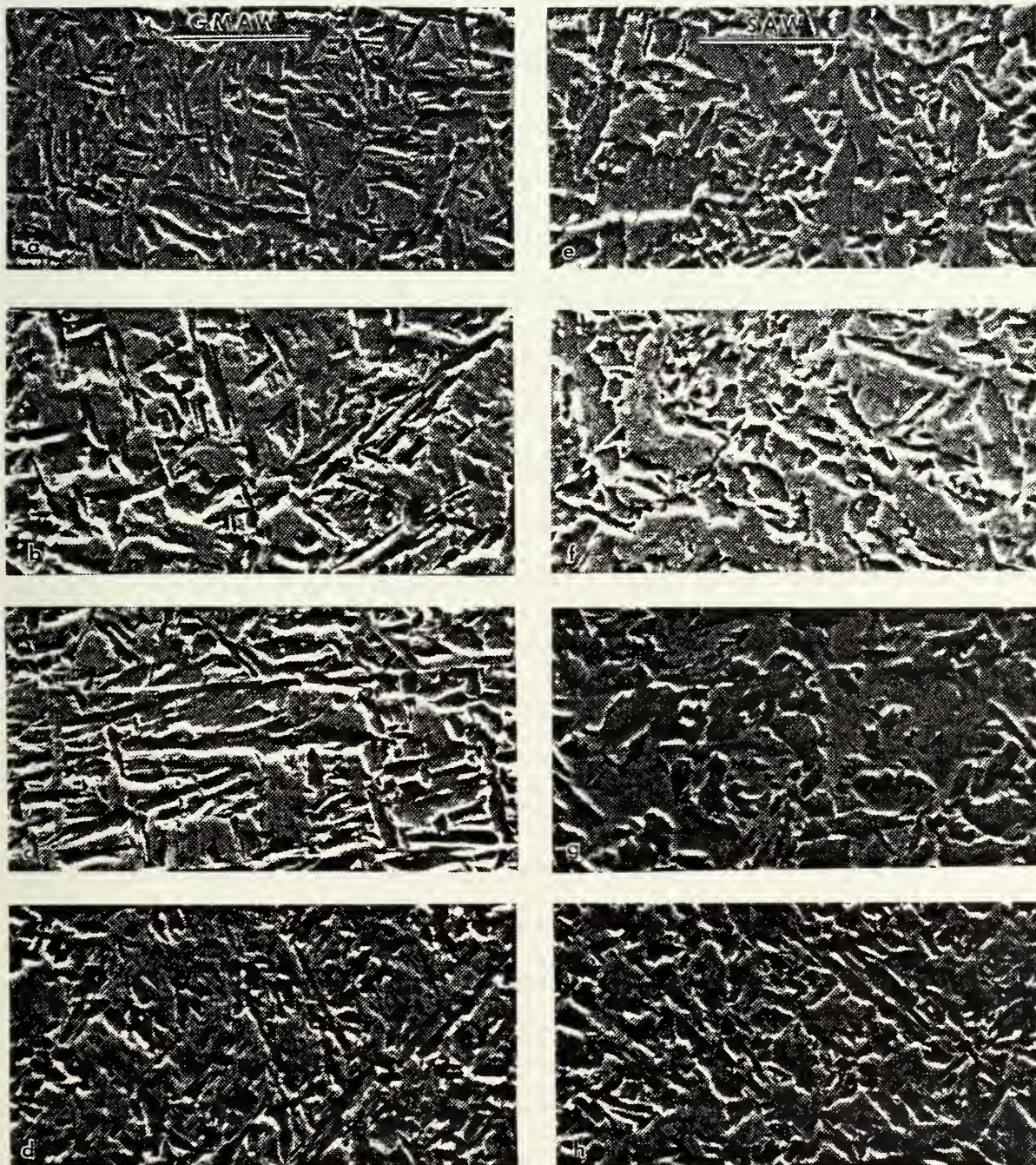


Figure 20 SEM micrographs of last pass in: (a, b, c and d) GMAW weld metal, fusion line, coarse-grained HAZ and fine-grained HAZ respectively, (e, f, g and h) SAW weld metal, fusion line, coarse-grained HAZ and fine-grained HAZ respectively.

4. Transmission Electron Microscopy (TEM)

Typical microstructures in the upper-weld region and in the weld metal coarse grained HAZ for each weldment are shown in Figures 21, 22 and 23. In the GMAW upper-weld region, typical microstructures include low carbon lath martensite, autotempered martensite, high dislocated martensite and some mixed B-II and B-III bainite.

In the SAW upper-weld region, microstructures are very different and typically include distributed carbide/cementite particle in ferrite matrix and laths. Carbide cementite particles are spherically shaped and are approximately 0.025 microns in diameter. Same lath martensite was observed but in general ferrite was the predominant microstructure. Bright and dark field micrographs exhibiting type II bainite with fine cementite particles distributed in ferrite laths are shown in Figure 22 along with corresponding SADP using a cementite diffraction spot.

In the GMAW coarse grained HAZ, typical microstructures include lath and small amounts of transformed twinned martensite with some B-III bainite.

In the SAW coarse grained HAZ typical microstructures include small martensite islands in highly dislocated ferrite matrix, and profuse distribution of carbide/cementite particles in ferrite matrix and are shown in Figure 23.

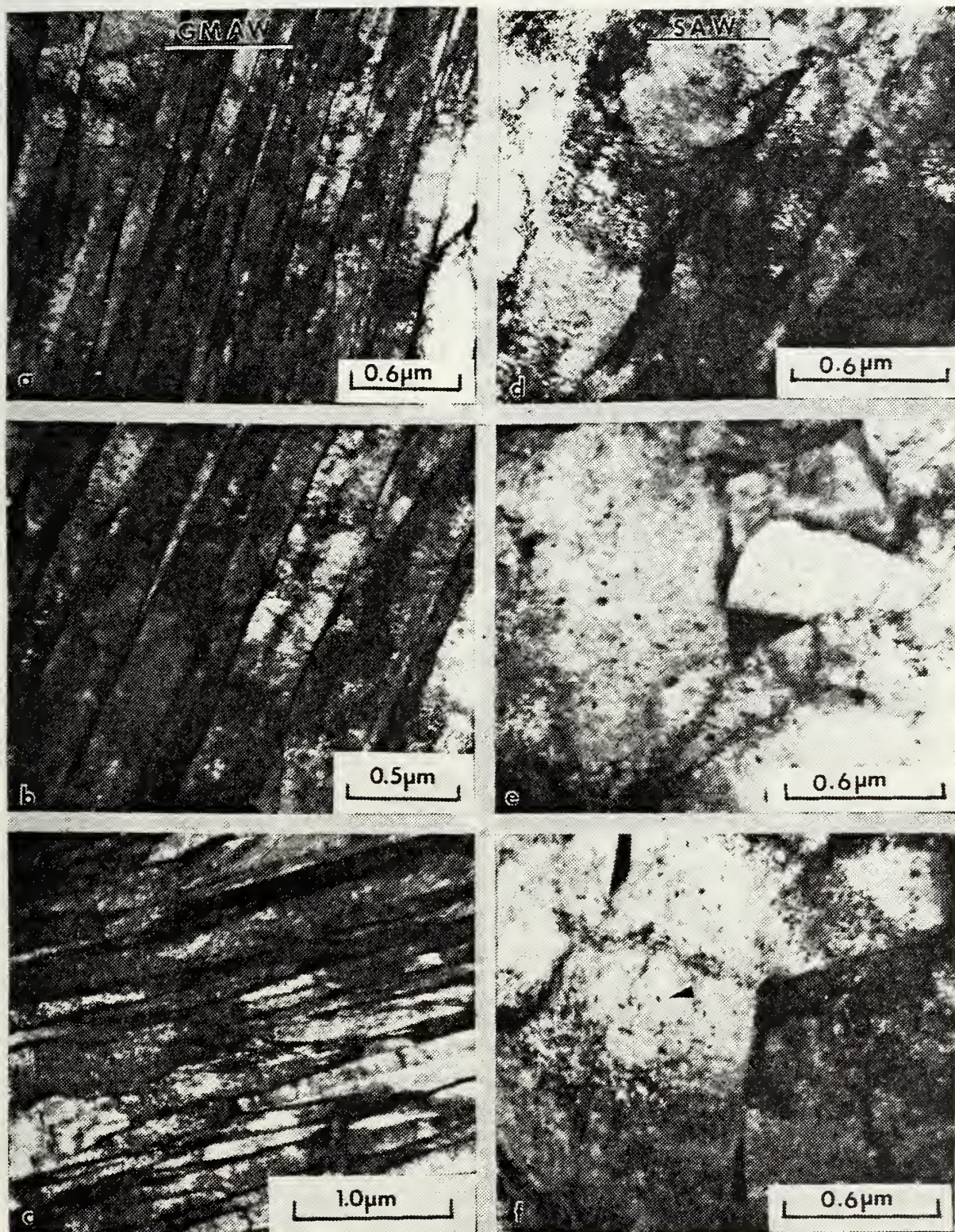


Figure 21 TEM micrographs in the last pass weld metal of GMAW and SAW weldments of HY-100 steel exhibit: (a, b and c) typical low carbon lath martensite, (d) lath martensite, (e) and (f) distribution of carbide/cementite particles in ferrite matrix.

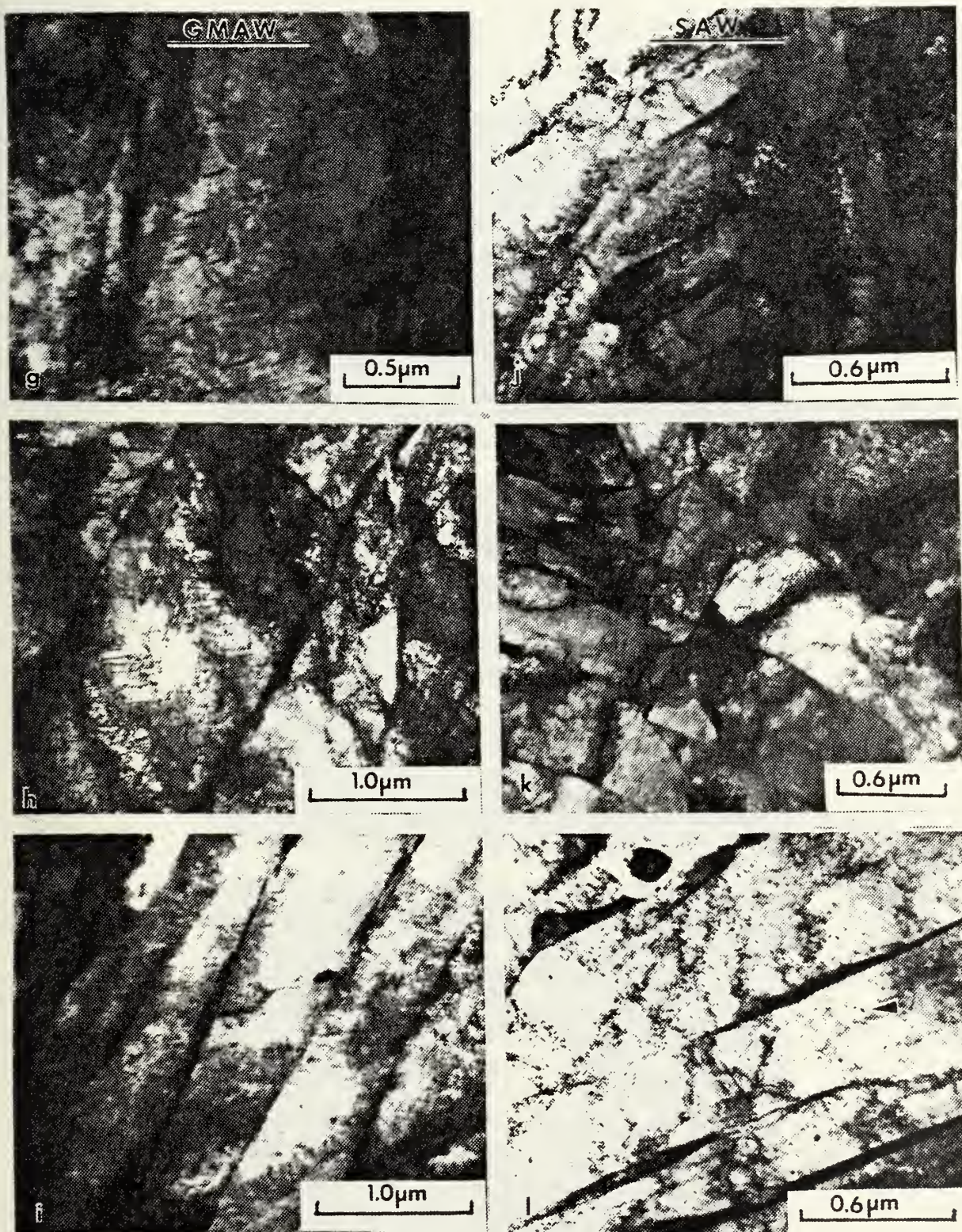


Figure 21 Continued TEM micrographs in the last pass weld metal of GMAW and SAW weldments exhibit: (g) autotempered martensite, (h) highly dislocated lath martensite, (i) mixed B-II and B-III bainites, (j) distribution of carbides/cementite in highly dislocated ferrite matrix, (k) subgrains of ferrite and (l) distribution of fine carbide/cementite particles in ferrite laths.

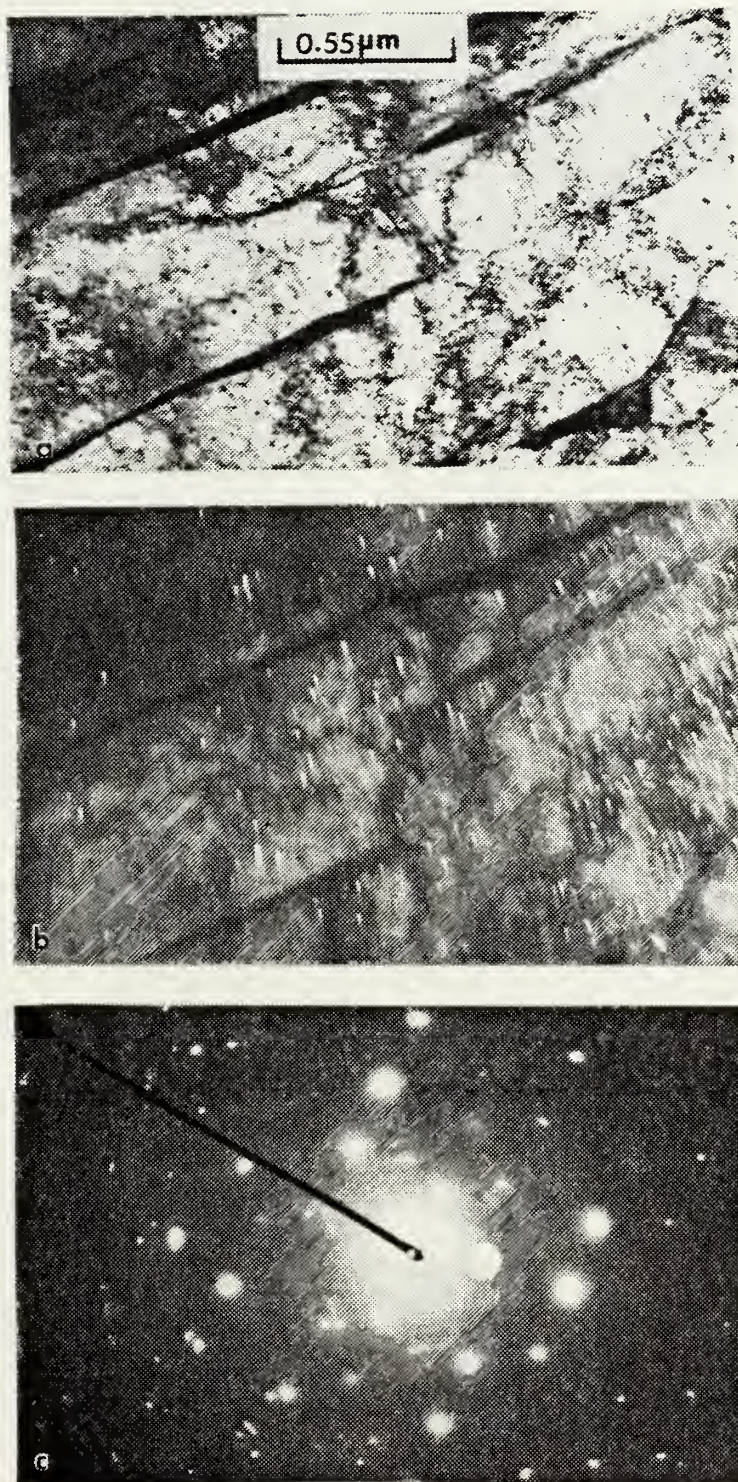


Figure 22 TEM micrograph of SAW upper weld region exhibiting type-II Bainite with fine cementite particles distributed in the ferrite laths: (a) bright field, (b) dark field and (c) corresponding SADP using cementite diffraction spot.

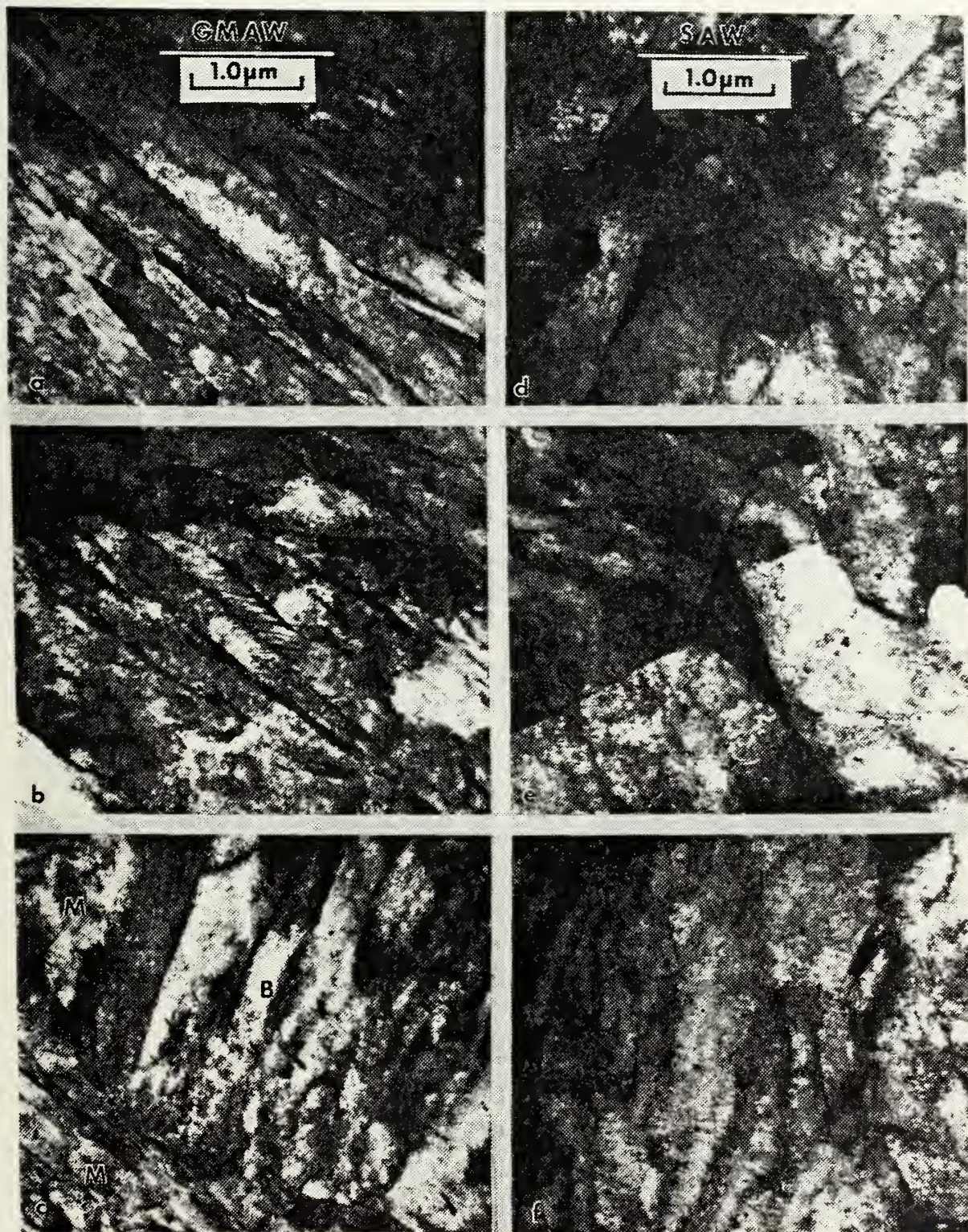


Figure 23 TEM micrographs of coarse-grain HAZ of last pass weld metal of GMAW and SAW weldments in HY-100 steel show: (a) typical lath martensite, (b) transformation twinned martensite, (c) B-III bainite with lath martensite, (d) small martensite island in highly dislocated ferrite matrix (e) small martensite island and distribution of carbide/cementite particles in ferrite matrix and (f) profuse distribution of carbide/cementite particles in ferrite matrix.

5. Fractography

SEM fractographs taken of fully ductile and brittle fractured surfaces are shown in Figures 24 and 25. No significant differences were noted in the fracture mechanics which could explain why the SAW weldment exhibited a marginally superior toughness at 60°C.

6. Weld Metal Chemical Composition

The results of the GMAW and SAW metal constituent analysis are presented in Table 5. The SAW weldment contained more oxygen than the GMAW weldment and the carbon content in both weldments appears to be high at 0.15%.

7. Weld Process Cooling Rates

For the GMAW weldment, the cooling rate in beads 7, 13, 16 and 17 were measured by the TC plunge techniques. The average cooling rate at 1000°F was 34°F/sec (see Figure 2).

For the SAW weldment, the cooling rate in beads 8, 11, 14, and 17 were also measured at 1000°F by the TC plunge technique. The average cooling rate was 20°F/sec, (see Figure 3).

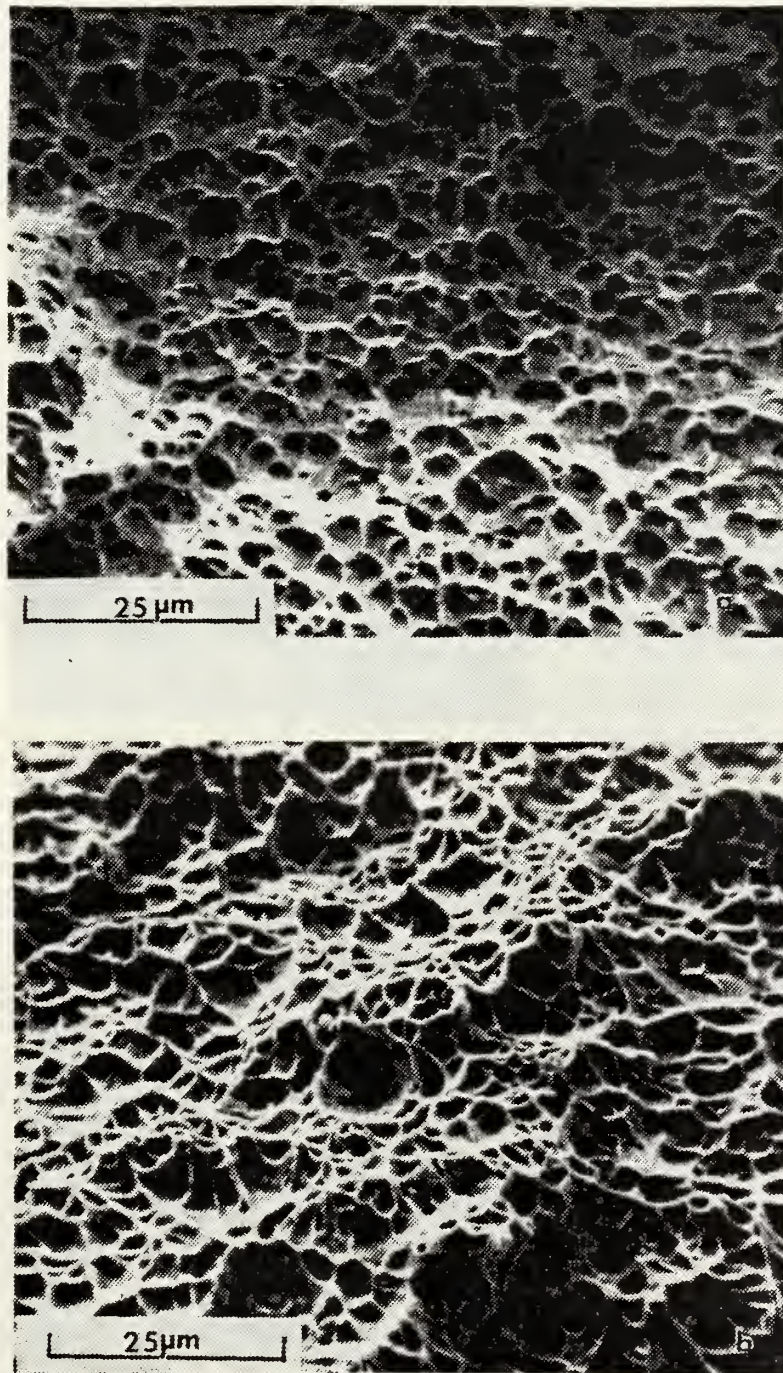


Figure 24 SEM micrographs of ductile fracture surface in
(a) GMAW (b) SAW. Specimens tested at 60°C.

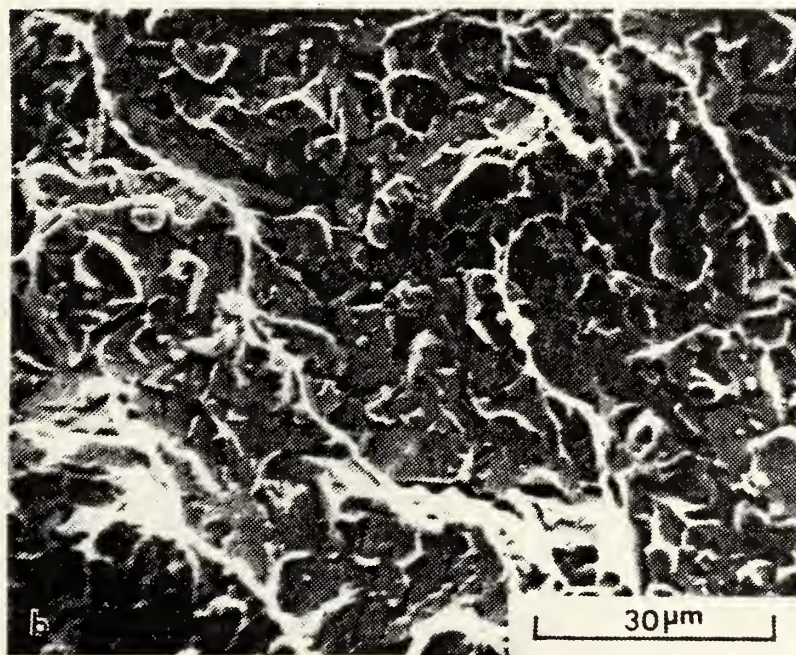
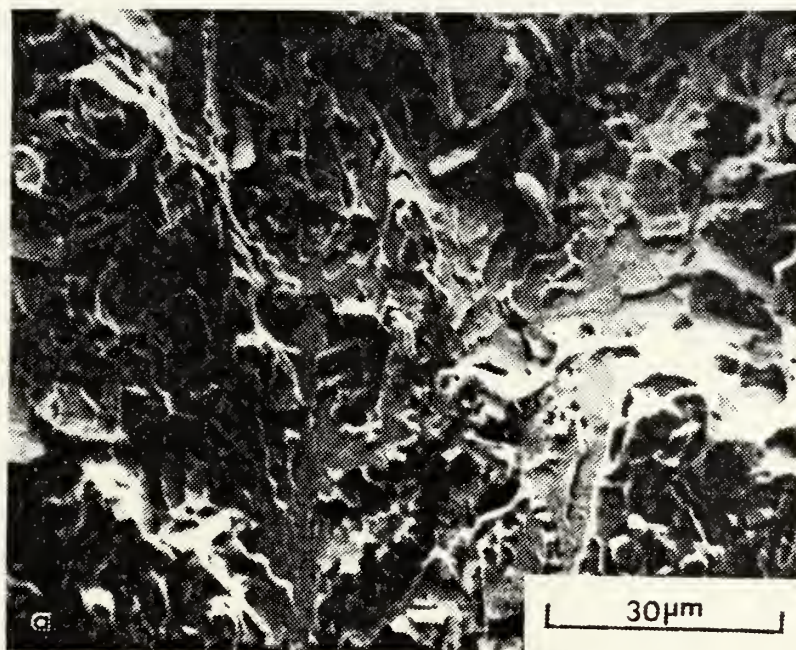


Figure 25 SEM micrographs of brittle fracture surface in
(a) GMAW (b) SAW. Specimens tested at -196°C .

Table 5

Chemical Composition of HY-100 GMAW and SAW Weldments

Element	GMAW (%)	SAW (%)
Carbon	0.15	0.15
Manganese	1.42	1.37
Silicon	0.26	0.33
Phosphorus	0.008	0.015
Sulphur	0.007	0.007
Nickel	2.52	2.51
Molybdenum	0.50	0.50
Chromium	0.38	0.39
Vanadium	0.00	0.00
Aluminum	0.00	0.00
Titanium	0.00	0.00
Zirconium	0.00	0.00
Copper	0.06	0.06
Oxygen	0.016	0.023
Nitrogen	0.008	0.007
Barium	<0.1	<0.1

V. DISCUSSION

It is desirable that the mechanical properties of the weldment equal or exceed those of the parent base metal. The impact requirements for HY-100 steel plate 1/2 inch thick and over [Ref. 3] are 45 ft-lbs at -84°C and 70 ft-lbs at -17°C . In the GMAW weldment Figure 13 these requirements are met or exceeded. However, the SAW weldment although exceeding the requirement at -17°C , falls far short of the requirement at -84°C .

It is interesting to note that the tempered weld metal hardnesses measured for both weldments, Figure 12, are approximately equal to about 250 HV. This is convenient for our analysis since the notch in the charpy impact specimens was placed at the center of each weldment so cracks would propagate through the center of the weld where the hardnesses have been shown to be about the same. Therefore the impact data developed for each weldment can be said to represent a comparison of toughnesses at a given hardness. So then, the difference in impact properties between weldments can be explained almost totally on the basis of the microstructures resulting from the welding thermal cycling.

The GMAW weldment exhibited primarily a fine lath martensitic structure (often autotempered) which in multipass weldments would be tempered producing the microstructure

recognized as providing the best resistance to brittle fracture. Its inclusion count was measured at 7,170 inclusions/mm². The SAW weldment on the other hand was observed to have blocky ferrite and upper bainite transformation products with carbide/cementite precipitates. This microstructure is generally associated with a decrease in the toughness in SAW weldments as reported in studies conducted by Abson and Dolby, [Ref. 7] and Ito and Nakanishi, [Ref. 8]. For the SAW weldment, an inclusion count of 9550 inclusions per mm² was measured. This represents about 25% more inclusions than measured in the GMAW.

As the microstructures developed in each weldment can be used to explain the ductile-to-brittle transition temperature (DBTT) differences observed the cooling rates and inclusion counts associated with each weld process can be used to explain, in part, the microstructures, (it is recognized that other factors can contribute to the type of transformation products observed in weldments). The GMAW process's significantly faster cooling rate (42%) and lower inclusion content would explain the fine lath martensite/ lower bainitic microstructure observed in this weldment. Conversely the SAW process's lower cooling rate and higher inclusion count would combine to explain the coarse upper bainitic microstructure observed in the SAW weldment. Every effort was made to maintain equal weld process parameters. Even the reported weld metal composition for each weldment

are very similar. With regard to the two major differences described above, the similarity in upper shelf impact energies of the weldments suggest that perhaps cooling rate and not inclusion distribution would be the major factor responsible for the microstructures and their resulting DBTT differences. If the opposite were true, the greater inclusion count in the SAW would be expected to result in a lower upper shelf energy vis-a-vis the GMAW since microvoid coalescence is a function of inclusion distribution. Nevertheless with the present data, it would be difficult to show that cooling rate is in fact dominant over inclusion count and vice-versa. It may be beneficial, however, to consider the effect each may have on the weld metal microstructure.

A. INCLUSIONS

Generally weld metal compositions containing higher oxygen and sulphur contents will contain a greater population of inclusions. This would have the effect of giving rise to microstructures consisting of higher transformation temperature products. Inclusions formed during the welding process play a significant but varying role in the fracture toughness properties associated with weldments of the various steels. Abson, D. J. and Dolby, R. E. [Ref. 9] in a study of the effects of non-metallic inclusions on ferrite nucleation in carbon steel weld metal, found that these inclusions

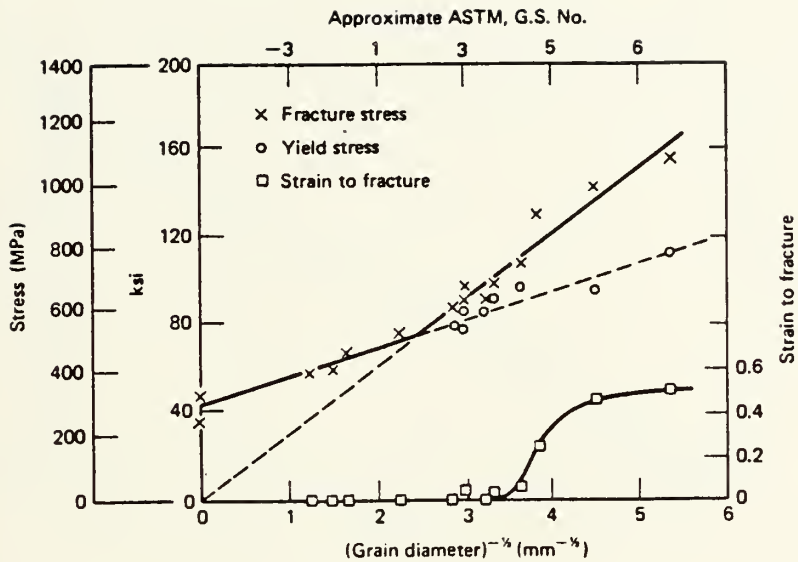
acted as nucleation sites for the formation of accicular ferrite. Accicular ferrite has been found in a previous study by Dolby, R. E., [Ref. 10] to be a microstructural constituent important for good weld toughness. In a study of carbon-manganese weld metals, Abson, D. J. and Dolby, R. E. [Ref. 11] concluded that weld metal in the intermediate oxygen regime (approximately 0.03%) exhibited the optimum distribution of inclusions necessary to maximize accicular ferrite nucleation. This suggests that in the less hardenable C-Mn weld metal, inclusions are not only desirable but necessary for good weld toughness.

Based on this information, it would seem appropriate to consider the effect on fracture toughness that a greater volume fraction of accicular ferrite would have in HY-100 SAW weldments. Levine and Hill [Ref. 12] in a study on the structure-property relationships in C-Mn weld metal, measured the impact toughness of a primarily accicular ferrite microstructure. The DBTT was determined to be at about -16°C . In this research the DBTT of the predominantly tempered martensitic microstructure of the GMAW weldment was determined to be about -70°C . This comparison suggests that improvements in fracture toughness in the HY-100 SAW weldments would not be realized if accicular ferrite were the dominant microstructure.

B. COOLING RATES

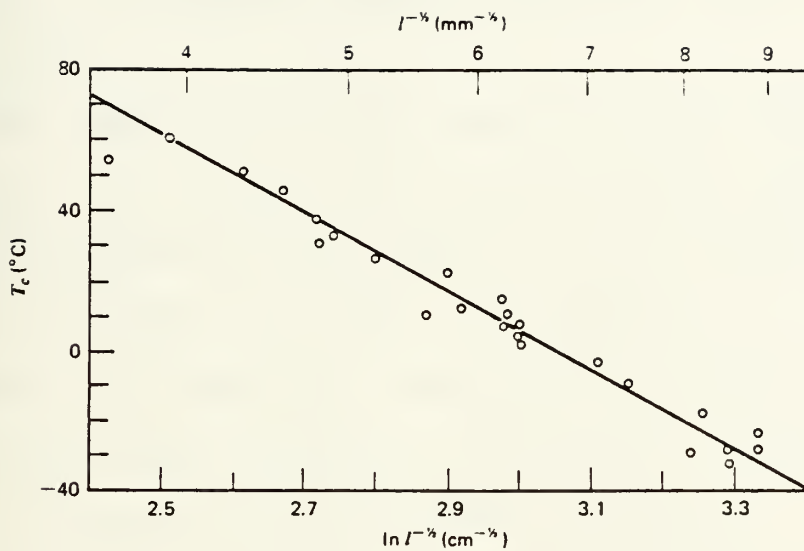
Increasing cooling rates is an ideal mechanism for introducing microstructural grain refinement. Microstructural refinement represents a unique opportunity by which the material may be both strengthened and toughened. This represents a particularly attractive strengthening mechanism in view of the generally observed inverse relationship between strength and toughness. One beneficial effect of grain refinement is a reduction in the DBTT. To explain this, it is only necessary to consider that a microcrack will be stopped by an effective barrier (the grain boundary) more often, the finer the grain size.

Figure 26 demonstrates that fracture stress is more sensitive to grain size than the associated yield strength. There are some important implications to be drawn from these data. First the intersection of the yield strength and fracture strength curves represents a transition in material response. For large grains (greater than critical size), failure must await the onset of plastic flow; hence, fracture occurs when yield strength equals fracture stress. For grains smaller than critical size, yielding occurs first and is followed by eventual failure after a certain amount of plastic flow--the amount increasing with decreasing grain size. The latter situation reflects greater toughness with an increasing ratio of fracture stress to yield stress. Since fracture stress and yield strength are temperature



Source: Published information in Reference [12]

Figure 26 Yield and Fracture Strength and Fracture Stain Dependence on Grain Size in Low Carbon Steel at -196°C



Source: Published information in Reference [12]

Figure 27 Dependence of Transition Temperature on Grain Size

sensitive properties, the critical grain size for the fracture transition would be expected to vary with test temperature. Consequently, the transition temperature is shown to decrease strongly with grain size as shown in Figure 27.

This effect in bainitic steels is supported by several studies. In a study of bainite and bainite-martensite duplex structures in low carbon low-alloy high strength steels, Kunitake et al [Ref. 14] showed that by lowering the austenite transformation temperature, nucleation sites for the bainite laths increased, effectively refining the bainite packet widths in all three types of bainites. This resulted in a lowering of the DBTT, thereby improving the toughness.

Naylor and Krake [REf. 15] in a study of the effect of upper bainite packet size on toughness in low carbon steels concluded that by increasing cooling rates, the average bainitic packet size was refined and impact properties were improved. Increasing cooling rates can generally be associated with low temperature transformation products with resulting increases in strength and decreases in toughness. However, Naylor and Krake were able to show that this effect is cancelled and actually increases in toughness were observed.

Ultimately it is desired to use very high heat inputs in the SAW process, perhaps even as high as 100 kJ/inch (3.9 kJ/mm) in order to realize maximum deposition rates.

The high heat inputs, however, will further decrease the cooling rates and increasingly higher temperature transformation products would result. A three-dimensional solution to the Rosenthal equation

$$\frac{dT}{dt} = 2\pi K \left(\frac{v}{Q}\right) (T - T_0)^2$$

$\frac{dT}{dt}$ - cooling rate

K - Thermal conductivity

v - welding velocity

Q - heat input rate

T - melting temperature

T₀ - preheat temperature

indicates that in the SAW process complete elimination of preheat would only increase the cooling rate by approximately 13% over that experienced with a preheat of 275°F (135°C). It is expected that significantly higher cooling rates would be required to lower austenite transformation temperatures into a regime where the higher toughness lower bainite-martensite duplex microstructure might become predominant.

Significantly increasing cooling rates with the high heat input SAW process seems to be the only practical course of action, if the high deposition rates required by the economics of modern-day shipbuilding are to be realized with the currently available filler metals.

VI. SUMMARY AND CONCLUSIONS

Based on the research and the results obtained, the following observations and conclusions can be made:

A. Gas Metal Arc Weldment

1. Average cooling rate was measured at 34°F/sec.
2. Inclusion count was 7,170 inclusions per square millimeter.
3. Tempered weld metal microhardness was 250 HV.
4. Last pass weld metal microhardness (untempered) was 300 HV.
5. The ductile-to-brittle transition temperature was -70°C.
6. Microstructure consisted primarily of lath martensite with some autotempered martensite.

B. Submerged Arc Weldment

1. Average cooling rate was measured at 20°F/sec.
2. Inclusion count was 9,550 inclusions per square millimeter.
3. Tempered weld metal microhardness was 250 HV.
4. Last pass weld metal microhardness (untempered) was 250 HV.
5. The ductile-to-brittle transition temperature was -20°C.
6. Microstructure consisted primarily of a coarse upper bainitic structure.

- C. The difference between the properties of the two welds is attributed to their difference in microstructure. The difference in microstructure is believed to be primarily due to the difference in cooling rate, but the effect of inclusion

distribution should not be ignored until further information is available.

VII. RECOMMENDATIONS

Based on the research conducted, the results obtained and the conclusions drawn, the following recommendations are offered:

1. Further research should be conducted to determine the effect on microstructure and fracture toughness that a change in inclusion distribution would have for SAW HY-100 weldments.
2. A similar study should be conducted to determine the effect on microstructure and toughness caused by varying cooling rates.

LIST OF REFERENCES

1. American Welding Society, Current Welding Processes, 1968, pp. 2-3.
2. Department of the Navy Military Specification MIL-S-19322, "Military Specification Fabrication, Welding and Inspection of HY-80/100 Submarine Hulls."
3. Department of the Navy Military Specification MIL-S-16216J (Ships), "Military Specification Steel Plate, Alloy, Structural, High Yield Strength [HY-80 and HY-100]," (15 March 1972).
4. Brick, R., Pense, A. and Gordon, R., Structure and Properties of Engineering Materials, McGraw Hill Book Company, 1977.
5. Emmanuel, G. N., Young, D. E., Spahr, G. L., "The Metallurgy of Weld Heat-Affected Zones in HY-80 High Strength Steel," Metals Engineering Quarterly 1(3), pp. 82-87 (1961).
6. Lancaster, J. R., Metallurgy of Welding, George Allen and Unwin, 1980, pp. 56-85.
7. Abson, D. J., Dolby, R. E. and Hart PHM, Investigation into the role of non-metallic inclusions on ferrite nucleation in carbon steel weld metals, Welding Institute Members Report 67/1978/M, 1978.
8. Ito, Y. and Nakanishi, M., "Study on Charpy Impact properties of weld metal with submerged arc welding," The Sumitomo Search, 1976 (15), May, pp. 42-62.
9. Abson, D. J., Dolby, R. E. and Hart PHM, Investigation into the role of non-metallic inclusions on ferrite nucleation in carbon steel weld metals, Welding Institute Members Report, 67/1978/M, 1978.
10. Dolby, R. E., Factors controlling weld toughness--the present position, Part 2--Weld metals, Welding Institute Members Report, 14/1976/M, 1976.
11. Abson, D. J. and Dolby, R. E., "Microstructural transformations in steel weld metals--a reappraisal," Welding Institute Research Bulletin, n.d.

12. Hertzberg, R. W., Deformation and Fracture Mechanics of Engineering Materials, pp. 326-328, Second Edition, John Wiley & Sons, 1976.
13. Levine, E. and Hill, D. C., "Structure-Property Relationship in Low Carbon Weld Metal," Metallurgical Transaction A, Volume 8A, September 1977.
14. Kunitake, Terrasaki F., Ohmori, Y., and Obtani, H., "The Bainite and the bainite-martensite duplex structure in low-carbon low-alloy high strength steels," Iron and Steel (UK), vol. 45, no. 6, 1972.
15. Naylor, J. P. and Krahe, P. R., "The Effect of the Bainite Packet Size on Toughness," Metallurgical Transactions, Vol. 5, July 1974.

INITIAL DISTRIBUTION LIST

	No. Copies
1. Defense Technical Information Center Cameron Station Alexandria, Virginia 22314	2
2. Library, Code 0142 Naval Postgraduate School Monterey, California 93943	2
3. Department Chairman, Code 69 Department of Mechanical Engineering Naval Postgraduate School Monterey, California 93943	1
4. Associate Professor K. D. Challenger, Code 69Ch Department of Mechanical Engineering Naval Postgraduate School Monterey, California 93943	5
5. Mr. Gene L. Franke, Code 2821 David Taylor Research Development Center Annapolis, Maryland 21402	1
6. Mr. Richard J. Wong, Code 2821 David Taylor Research and Development Center Annapolis, Maryland 21402	1
7. Mr. C. Zanis, Code 2821 David Taylor Research and Development Center Annapolis, Maryland 21402	1
8. Dr. Hans Vanderveldt Ship Systems and Technology NAVSEA Washington, D.C. 20362	1
9. LCDR Alfred E. Therrien, USN c/o R. A. Therrien 76 Saint Croix Street Lewiston, Maine 04240	2

207766

Thesis
T364
c.1

Therrien

Characterization of
submerged-arc and gas-
metal-arc weldments in
HY-100 steel.

25 OCT 88
13 APR 90

33538
35755

207766

Thesis
T364
c.1

Therrien

Characterization of
submerged-arc and gas-
metal-arc weldments in
HY-100 steel.



thesT364

Characterization of submerged-arc and ga



3 2768 002 03473 8

DUDLEY KNOX LIBRARY